Investigation of organic matter and biomarkers from Diepkloof Rock Shelter, South Africa: insights into Middle Stone Age site usage and palaeoclimate

James A. Collins[1*], Andrew S. Carr[2], Enno Schefuß[3], Arnoud Boom[2], Judith Sealy[4]

1) Alfred Wegener Institute for Polar and Marine Research, Am Alten Hafen 26, D-27568 Bremerhaven, Germany

2) Department of Geography, University of Leicester, University Road, Leicester LE1 7RH, UK

3) MARUM – Center for Marine Environmental Sciences, University of Bremen, Leobener Strasse 8, D-28359 Bremen, Germany

4) Department of Archaeology, University of Cape Town, Private Bag X3, Rondebosch 7701 South Africa

* Now at: GFZ-German Research Centre for Geosciences, Section 5.1 Geomorphology, Telegrafenberg, Potsdam 14473, Germany

Abstract

Diepkloof Rock Shelter (DRS) represents a site of major interest for reconstructing early human behaviours during the Middle Stone Age (MSA). Rock shelters such as DRS also potentially preserve information concerning the environmental context for such behaviours. In this respect the organic matter composition of rock shelter sediments has rarely been investigated in detail,

particularly at the molecular level. Here, we used pyrolysis-gas chromatography/mass spectrometry (py-GC/MS) to systematically assess the organic matter composition of bulk sediments within the MSA and Later Stone Age (LSA) sequence at DRS. From this we sought to gain insights into site usage, taphonomy and burning practices. Additionally, we analyzed the chain length distribution of leaf-wax *n*-alkanes as well as their hydrogen and carbon isotopic compositions (δD_{wax} and $\delta^{13}C_{wax}$) to investigate their potential as hydroclimate and vegetation indicators. This constitutes the first leaf-wax isotopic data in a terrestrial context of this antiquity in South Africa.

Py-GC/MS shows a dichotomy between stratigraphic units (SUs) of high organic matter content, producing a range of pyrolysis products, including homologous series of long chain *n*-alkene/*n*-alkane doublets and alkyl-nitriles, and SUs of low organic matter content, dominated by aromatic, heterocyclic N and polycyclic aromatic hydrocarbon (PAH) pyrolysis products; typical molecular burning products. Several SUs of the Intermediate Howiesons Poort interval exhibit the latter composition, consistent with micromorphological evidence.

$\delta^{13}C_{wax}$ remains stable throughout the MSA, but leaf-wax *n*-alkane chain length and δD_{wax} increase during the Late Howiesons Poort interval. Comparison with such patterns in modern plants in the region suggests this represents a shift towards the input of more arid-adapted vegetation into the shelter, driven either by aridification in site locale or a change in selection practices. Our results suggest that these techniques have potential at other sites in southern Africa and globally where organic matter preservation is high.

Key words

Organic matter composition, py-GC/MS, $\delta^{13}C_{wax}$, δD_{wax}, PAHs, *n*-alkane chain length distribution, burning

1. Introduction

Diepkloof Rock Shelter (DRS), Western Cape Province, South Africa (**Fig. 1**) hosts a sequence spanning the pre-Still Bay to Howiesons Poort industries of the Middle Stone Age (MSA), and is overlain by Later Stone Age deposits (LSA; Porraz et al., 2013; **Fig. 2a**). The site has yielded a multitude of findings, including lithic artefacts (Porraz et al., 2013), charcoal remains (Cartwright, 2013; Miller et al., 2013), specific hafting residues (Charrié-Duhaut et al., 2013), ochre (Dayet et al., 2013) and faunal remains (Steele and Klein, 2013). Perhaps the most remarkable finding is the earliest evidence for engraved ostrich eggshell (EOES) during the Early Howiesons Poort interval (Texier et al., 2013), thought to represent a significant cultural and social development (Texier et al., 2010). Developing an environmental context for such cultural/social developments, both at DRS and beyond (e.g. Henshilwood et al., 2002) has, however, proved challenging in this locale and on the wider southern Cape (Chase, 2010), fundamentally reflecting the lack of contemporaneous terrestrial environmental archives (Carr et al., 2016b).

Faunal remains and stone tool assemblages from MSA sites often provide valuable archaeological and environmental insights. However, it has been noted that there is often relatively limited consideration of the organic material within many MSA deposits (Wadley, 2015). In cases where organic material has been

71 directly analysed, striking insights have been provided, including identification
72 of bedding structures (Goldberg et al., 2009; Wadley, 2011) and specific
73 geochemical evidence for the use of chemical adhesives (Charrié-Duhaut et al.,
74 2013). Here we consider the molecular character of sedimentary organic matter
75 in an archaeological context both to support archaeological inference and to gain
76 insights into environmental change. We specifically aim to investigate questions
77 surrounding the degree of burning, the types of vegetation brought into the site
78 and evidence for past hydroclimatic change. We characterize the organic
79 composition of the sediments and assess the degree to which each stratigraphic
80 unit was burnt using pyrolysis-gas chromatography/mass spectrometry (py-
81 GC/MS), while vegetation type and hydroclimate are considered via the
82 distribution and isotopic composition of leaf-wax *n*-alkanes.

83 ## 2. Diepkloof Rock Shelter background and setting

84 ### 2.1 Setting and stratigraphy

85 DRS is located at ~120m altitude above the Verlorenvlei wetland about 14km
86 from the modern coastline. The rock shelter formed within a quarzitic sandstone
87 butte, and has a floor area of 200m^2. Based on stone tool assemblages, the
88 sedimentary sequence within the shelter has been ascribed to different techno-
89 cultural phases of the MSA (Porraz et al., 2013). From bottom to top the complete
90 sequence includes the Lower MSA, MSA 'Mike', pre-Still Bay, Still Bay, Early
91 Howiesons Poort, MSA 'Jack', Intermediate and Late Howiesons Poort and finally
92 the post-Howiesons Poort (Porraz et al., 2013); here we focus on the pre-Still Bay
93 to Late Howiesons Poort (**Fig. 2**). The sequence has been further divided into
94 Stratigraphic Units (SUs), which represent complexes of individual lenses and

beds (microfacies; Miller et al., 2013), given names ordered mainly alphabetically from the top to the base.

Micromorphological analysis indicates that the sediments in the rockshelter comprise ash, charcoal and siliciclastic fragments, as well as bone, eggshell, and humified organic remains (Miller et al., 2013). The upper part of the section, corresponding to the Intermediate and Late Howiesons Poort, displays evidence for the raking out of hearths and the burning of bedding, suggesting more frequent or intensive site use (Miller et al., 2013).

In terms of palaeoclimate and palaeovegetation, charcoal remains indicate variability in the vegetation brought to the shelter between the Still Bay and Howiesons Poort (Cartwright, 2013). During the Still Bay, the charcoal assemblage comprises a range of both Afromontane forest and thicket taxa, while during the Howiesons Poort, vegetation indicates a wider range of taxa, including more thicket and shrubland woody taxa, implying a shift towards more arid conditions (Cartwright, 2013). Faunal remains have also yielded insights into the past vegetation of the region. Evidence for grazers, rare during the LSA, was taken to indicate that more grassy conditions prevailed during the MSA relative to the LSA (Steele and Klein, 2013), although in this context the exposed continental shelf, which was up to ~20km in extent during the period of MSA occupation (Porraz et al., 2013), may account for some changes in faunal assemblage.

Given that vegetation brought to the site was selected by the inhabitants and represents only a specific fraction of the vegetation surrounding the site, it is also plausible that the above changes in vegetation and faunal assemblage reflect changes in selection practises by the inhabitants. Nonetheless, it may be argued that on these long timescales, climate is the overarching control on the available vegetation. Either way, this represents an important aspect to bear in mind when interpreting our data.

2.2 Chronology of the DRS sequence

The LSA sequence at DRS is believed to span the last 1.8 ka (Parkington and Poggenpoel, 1987). For the MSA sequence, two different optically stimulated luminescence (OSL) chronologies have been proposed. The initial chronology from grid squares C6 and L6 within the shelter (Jacobs and Roberts, 2015; Jacobs et al., 2008) indicated that the Still Bay to Late Howiesons Poort industries span an age range of 73.6 ± 2.5 ka to 60.5 ± 1.9 ka. Later studies using both thermoluminescence and single grain OSL (Feathers, 2015; Tribolo et al., 2013; Tribolo et al., 2009) from grid squares M7, N7, L6 and M6 and P11-Q11 (for OB2-4) suggest that the Still Bay to Late Howiesons Poort spans an age range between 109 ± 10 ka to 52 ± 5 ka and tend to be clustered, with the Still Bay (109 ± 10 ka) producing a similar age to the Early Howiesons Poort (105 ± 10 ka to 109 ± 10 ka) and the Intermediate Howiesons Poort dated at 85 ± 9 ka to 77 ± 8 ka. The late Howiesons Poort is much younger (52 ± 5 ka), although this is taken from the back sector of the excavation (Tribolo et al., 2013). The disparities in these chronologies are yet to be resolved (Jacobs and Roberts 2015, Feathers 2015). As some dated samples were obtained from different grid squares of the site these

differences may reflect some as yet undiscerned stratigraphic complexity at the site. As such, because our samples were taken closest to material analysed by Tribolo et al., (2013), we refer to their ages.

2.3 Climate and vegetation of the region

The locale around DRS comprises a mosaic of vegetation (Cartwright 2013). Briefly, steep rocky kloofs (ravines) provide shelter and retain enough soil moisture to permit growth of some occasional trees and mesic thicket taxa including small trees and shrubs. Going downslope from the shelter, crevices and large boulders retain enough moisture to permit growth of thicket, while further downslope, sandy soils favour the growth of asteraceous shrubs, seasonal bulbs, succulents and grasses.

DRS is positioned within the Lowland Fynbos biome, just south of the boundary with the Succulent Karoo biome (**Fig. 1a**). The Fynbos biome (comprising the Lowland and Montane Fynbos eco-regions), which extends to the southwest of DRS is a Mediterranean-type shrubland comprising sclerophyllous proteoid shrubs, small-leaved ericoid shrubs (notably from the Ericaceae family), Cape reeds (Restionaceae) and various geophytes from the Liliaceae and Iridaceae families (Cowling et al., 1997). The vegetation of the Fynbos biome is characterised by a general absence of trees and adaptation to summer drought. There are a small number of CAM species, but most plants use the C_3 pathway (Vogel et al., 1978). Some halophytic C_4 vegetation occurs on the banks of the Verlorenvlei wetland (Carr et al., 2015). DRS receives ~250 mm of precipitation per year, which is delivered mostly (70%) during austral winter. Regions south

and west of DRS are less arid (**Fig. 1b**) and receive 200-500 mm of precipitation per year, delivered mainly (70-90%) during winter.

The Succulent Karoo biome (**Fig. 1a**) to the north of DRS is characterised by a generally hotter and more arid climate (**Fig. 1b**), particularly during the summer, and the biome comprises more drought-adapted species such as leaf succulents and dwarf shrubs from the Aizoaceae, Crassulaceae and Euphorbiaceae families (Milton et al., 1997). Many species in the Succulent Karoo use CAM photosynthesis (Rundel et al., 1999) and are characterised by thick, waxy cuticles, dwarf succulence and shallow rooting systems. In the northern Succulent Karoo, mean annual rainfall is approximately 150-300 mm yr^{-1} (Hijmans et al., 2005), and seasonality is markedly reduced (~50% during the winter).

3. Background to the organic matter and molecular approach

3.1 Rockshelter organic matter composition

Micromorphological analyses suggest terrestrial plants represent a significant component of the organic material preserved in rockshelter sediments (Miller et al. 2013), along with burning products, be they derived originally from plants (Cartwright, 2013) or animal products (Goldberg et al., 2009; Miller et al., 2013). The major organic components of fresh vegetation include macromolecular lignin, cellulose and leaf cuticles (e.g. cutin macromolecule); the latter is also associated with the synthesis of soluble leaf waxes. While cellulose has a low preservation potential in the arid environments of southern Africa (Carr et al., 2010; 2013), sedimentary lignin monomers can be used to reconstruct past

191 vegetation types (Goñi and Hedges, 1992), although their preservation can be
192 variable (Thevenot et al., 2010). Leaf-wax lipids, particularly *n*-alkanes, tend to
193 be relatively well preserved in a variety of sedimentary contexts and are
194 preserved within soils throughout the study area (Carr et al., 2014).
195
196 Incomplete or variable combustion of organic matter, as would be anticipated in
197 an archaeological context, generates a continuum of organic materials (Masiello,
198 2004), with more prolonged burning or higher temperatures producing organic
199 matter increasingly dominated by PAHs, and other aromatic compounds
200 characterised by the presence of more ring structures (e.g. Simoneit, 2002).
201
202 To assess the organic matter composition of DRS sediments we use py-GC/MS,
203 which can be performed directly on sediments, without extraction. Pyrolysis
204 thermally fragments macromolecules in an inert atmosphere, rendering large
205 macromolecular compounds (such as cellulose and lignin) amenable to GC
206 analysis (e.g. Sáiz-Jiménez and De Leeuw, 1986). Our aims are to compare the
207 organic matter components preserved in the MSA (late Pleistocene) and LSA
208 (late Holocene) sediments and to identify whether burning indicators (e.g. PAHs)
209 relative to unburnt compounds (e.g. leaf waxes) change through the sequence
210 and how this relates to other cultural/societal changes.

211 ### 3.2 Leaf-wax *n*-alkanes

212 We also analysed leaf-wax *n*-alkanes, which are commonly utilized in
213 palaeoenvironmental research, given their suitability for compound-specific
214 hydrogen and carbon isotopic analysis (Eglinton and Eglinton, 2008). Leaf-wax

derived *n*-alkanes are typically long-chain compounds, with a chain length distribution between about 25 and 33 carbon atoms (C_{25}-C_{33}) and a strong tendency for odd/even chain length preference (Eglinton and Hamilton, 1967).

The chain-length distribution of leaf-wax *n*-alkanes can provide information regarding vegetation type (e.g. Poynter et al., 1989; Vogts et al., 2009). In the Western Cape, the *n*-alkane distributions from the Fynbos biome are, on average, distinct from those of the Succulent Karoo (Carr et al., 2014). Fynbos vegetation tends to be C_{31} and C_{29} dominated while Succulent Karoo vegetation tends to be dominated by *n*-alkanes of C_{31} and C_{33} chain length (**Fig. 3a**), which likely reflects the combined effects of a more arid climate and the associated transition to more drought-adapted plants within the Succulent Karoo biome. This feature of the chain length distribution is typically summarized (Carr et al., 2014; Schefuß et al., 2003) using the Norm31 index ($C_{31}/C_{31}+C_{29}$). Vegetation of the Lowland Fynbos biome is thus characterized by lower Norm31 values (mean of 0.57 ± 0.31, n=28) than the Succulent Karoo (mean of 0.84 ± 0.17; n=133; **Fig. 1a;** Carr et al., 2014; Herrmann et al., 2016).

Compared to soils and sedimentary environments, there are additional factors affecting leaf-wax preservation within an archaeological site. Laboratory and field burning experiments show that incomplete combustion of leaf waxes increases the proportion of shorter chain length and even-numbered *n*-alkanes due to fragmentation of the longer homologues, with greater fragmentation occurring with higher combustion temperatures (Eckmeier and Wiesenberg, 2009; Mallol et al., 2013; Wiesenberg et al., 2009). The *n*-alkane average chain

length (ACL_{14-35}) of maize straw dropped from 30.2 to 25.8 when burnt at 300°C and to 17.4 at 500°C (Wiesenberg et al., 2009). The odd-over-even number preference of the waxes, summarised by the carbon preference index (CPI_{27-33}, where values around 1 indicate no odd-over-even preference), was reduced from 10.7 when unburnt, to 2.6 at 300°C and then 0.9 at 500°C (Eckmeier and Wiesenberg, 2009; Wiesenberg et al., 2009).

We aim to determine to what degree the leaf-wax chain-length distribution of DRS sediments reflects the primary vegetation versus combustion processes and whether the Norm31 index can elucidate past changes in vegetation input.

3.3 Leaf-wax isotopes (δD_{wax} and $\delta^{13}C_{wax}$)

δD_{wax} is commonly utilized as a palaeohydrological indicator. Precipitation is the ultimate source of hydrogen for leaf waxes and δD_{wax} typically records changes in precipitation δD (δD_p; Sachse et al., 2012), which in turn reflects precipitation source and/or amount (Rozanski et al., 1993). Relative humidity and plant type exert secondary effects on δD_{wax} (Sachse et al., 2012).

The potential of δD_{wax} analysis in the Western Cape was demonstrated by Herrmann et al., (2017), who showed reasonably coherent changes in δD_{wax} with aridity for contemporary soils from across the sub-continent **(Fig. 1b)**. Higher δD_{wax} in the Succulent Karoo biome likely reflects lower precipitation amounts and increased evapotranspiration associated with long dry summers. The Western Cape (broadly, winter rainfall zone), however, displays a complicated

spatial pattern, possibly due to the effects of both summer and winter rainfall, the existence of microclimates and a diverse array of vegetation types in this mountainous region (Herrmann et al., 2017).

$\delta^{13}C_{wax}$ is a function of photosynthetic pathway and aridity, and is commonly interpreted as a palaeovegetation indicator. C_3 plants from the Succulent Karoo exhibit mean $\delta^{13}C_{wax}$ values of -34.2‰ ± 4‰ for the C_{31} *n*-alkane (Boom et al., 2014). CAM plants from the Succulent Karoo display higher but also more variable values (a mean C_{31} *n*-alkane $\delta^{13}C_{wax}$ value of -22.7‰ ± 6‰), with facultative CAM plants displaying a mean of -28.9‰ ± 3‰ (Boom et al., 2014). C_4 grasses exhibit an average C_{31} *n*-alkane $\delta^{13}C_{wax}$ value of -21.8‰ ± 2‰ (Rommerskirchen et al., 2006). The transect of southern African soils (Herrmann et al., 2016) displays an increase in $\delta^{13}C_{wax}$ in the Succulent Karoo to the NE of the study site.

The effect of burning or heating of *n*-alkanes might potentially affect δD_{wax} and $\delta^{13}C_{wax}$ values. Bulk plant $\delta^{13}C$ values display isotopic enrichment (~1 ‰) after burning (Poole et al., 2002), related to preferential loss of isotopically depleted components. Previous compound-specific work on this topic is limited, although it has been shown that mid-chain length fatty acids from aerosols produced during burning exhibit both increased and decreased $\delta^{13}C$ values, depending on the plant type (Ballentine et al., 1998), and thus reveal no systematic effect. It is thought that the mid-chain length compounds formed from chemical degradation during burning and the isotopic composition of the precursor molecules varies between plant types. This process is, however, unlikely to apply

289 to long-chain leaf waxes such as the C_{31} *n*-alkane, which likely represent the
290 intact original compounds.
291
292 At DRS we aim to investigate whether the leaf-wax isotopic composition reflects
293 the primary vegetation and hydroclimate signals or has been overprinted by
294 burning processes. Moreover, we aim to elucidate how vegetation, hydroclimate
295 and/or human selection practices have changed over time.

296 ## 4. Methods

297 ### 4.1 Sampling

298 Sediment samples were collected during the field season of 2013. Samples were
299 taken from the standing section. Sediment on the exposed surface was scraped
300 away, and the immediately underlying sediment scraped into glass vials using a
301 metal spoon that was wiped clean between samples. Samples from the MSA
302 levels were taken in grid square M7B, adjacent to the location of samples for
303 micromorphological analysis reported by Miller et al., (2013). Thirty-one
304 samples were taken in total, spanning SUs Lynn to Debbie (**Fig. 2**). This includes
305 two samples from each of SUs Eve, Frans and Leo to assess the variability within
306 individual SUs. LSA deposits were not preserved in this area of the site, so three
307 LSA samples were taken where deposits of this age were exposed. LSA 1 came
308 from the C6/C7 profile. LSA 2 was taken from the M5/M4 profile, in
309 approximately the middle of the square. LSA 3 came from the E6/E5 profile. Most
310 of the LSA deposits at Diepkloof occur as pits dug into the MSA layers. While
311 every effort was made to ensure that the LSA samples consisted of pit infill, it is
312 impossible to be certain that there is no admixture of MSA sediments.

4.2 Bulk parameters (%TC, bulk $\delta^{13}C_{TC}$, %TN and bulk $\delta^{15}N$)

In addition to the molecular indicators, we also analyzed bulk parameters. Bulk measurements of total carbon (%TC; including black carbon and organic carbon), bulk $\delta^{13}C_{TC}$, total nitrogen (%TN) and bulk $\delta^{15}N$ were determined at the University of Cape Town, after pre-treatment with 1M hydrochloric acid to remove carbonates. Samples were combusted at 1020°C in a Flash 2000 elemental analyser and the resultant gases analysed with a Delta V Plus isotope ratio mass spectrometer (ThermoScientific, Germany). Duplicate analyses of homogeneous material yielded a typical precision of 0.2‰ for both carbon and nitrogen isotopic measurements.

4.3 Pyrolysis-Gas Chromatography/Mass Spectrometry (py-GC/MS)

For py-GC/MS we analysed a subset of twenty MSA samples and all three LSA samples. Py-GC/MS was performed using a CDS1000 pyroprobe interfaced with a Perkin Elmer Clarus 500 GC/MS system. 25-50 mg of dried sediment (not previously solvent extracted) was encapsulated in a quartz tube, rested in the pyrolysis interface (at 300°C for 3 min) to minimise the inclusion of evaporated compounds (Sáiz-Jiménez, 1994), and then pyrolysed at 610 °C for 15 s. Gas chromatography was carried out using a CP-Sil 5CB MS column (30 m × 0.25 mm × 0.32 µm). The GC temperature programme began at 40 °C (1.8 min), was ramped to a final temperature of 310 °C at 4 °C min^{-1} and held for a further 20 min. Compounds within the pyrograms were identified based on their mass spectra and retention times (e.g. **Fig. 5**). Peak integrations were performed using the Turbo-Mass 5.2.0 software.

337 The relative proportion of each compound was determined using the summed
338 integrations for all identified compounds (up to a total of 148) in each pyrogram
339 (e.g. Carr et al., 2010b; Vancampenhout et al., 2008). Each compound was
340 classified into one of eight categories (e.g. Kaal et al., 2007) comprising: 1)
341 aliphatics (*n*-alkanes, *n*-alkenes, fatty acids); 2) nitrogen-containing compounds,
342 dominated by alkyl nitriles, but also associated with 3) some heterocyclic
343 aromatic moieties, such as (*n*-methyl) pyrole, pyridine, and quinoline; 4)
344 aromatics (e.g. benzene, xylene and alkylbenzenes); 5) polycyclic aromatic
345 hydrocarbons (PAHs; (n-methyl) naphthalene, biphenyl, (n-methyl) fluorene,
346 anthracene); 6) lignin pyrolysis products (known products of coniferyl, syringyl,
347 and coumaryl moieties); 7) phenolic compounds (e.g. phenol and methyl
348 phenols); 8) polysaccharide products (primarily furans and levoglucosan).
349
350 To provide further insight into the most probable macromolecular structures
351 and precursor compounds, pyrolysis was performed on three samples (LSA 1,
352 Logan and Ester) in the presence of tetramethylammonium hydroxide (TMAH)
353 (Challinor, 2001; Del Rio and Hatcher, 1998). This procedure, known as
354 thermally assisted hydrolysis and methylation, limits the degree of
355 fragmentation during pyrolysis and is also capable of transmethylation of ester
356 bonds; hence it depolymerizes important biopolyesters such as cutin.

357 ### 4.4 Leaf-wax extraction, purification and quantification

358 For leaf wax analysis, we extracted all thirty-one MSA samples. 2.6g to 5.8g of
359 dried sediment were extracted using an DIONEX ASE350 accelerated solvent
360 extractor at 100°C using a solvent mix of DCM:MeOH (2:1) for 5 minutes

repeated 3 times. The apolar fraction containing *n*-alkanes was obtained by elution of the dried lipid extract with hexane over a silica gel column (mesh size 60) followed by subsequent elution with hexane over $AgNO_3$ to remove unsaturated compounds.

n-Alkanes were identified using GC-FID, by comparison of retention times with an external standard mix. Squalane internal standard added before extraction yielded variable extraction recoveries, likely due to adsorption onto the complex organic matrix. We quantified *n*-alkane amounts by comparison with an external standard. Based on repeated analyses of an external alkane standard the quantification precision is <5%. We characterised the *n*-alkane distribution using standard parameters $CPI_{25\text{-}33}$, $ACL_{14\text{-}35}$ and Norm31 (following e.g. Carr et al., 2014, and references therein).

4.5 Leaf-wax isotopic analyses

$\delta^{13}C_{wax}$ was analysed using a ThermoFischer Scientific Trace Gas Chromatograph coupled to a Finnigan MAT 252 isotope ratio monitoring mass spectrometer (GC-IRMS) via a combustion interface operated at 1000°C. Isotope values were calibrated against external CO_2 reference gas and are reported in ‰ relative to VPDB. Samples were run in duplicate, with an average reproducibility of 0.1‰ for the C_{31} *n*-alkane. Leaf-wax *n*-alkane δD_{wax} was measured using a ThermoFisher Scientific Trace GC coupled, via a pyrolysis reactor operated at 1420°C, to a ThermoFisher MAT 253 isotope ratio mass spectrometer. δD values were calibrated against external H_2 reference gas and are reported in ‰ relative to VSMOW. Samples were analysed in duplicate with an average reproducibility

of 1‰ for the C_{31} *n*-alkane. Repeated analysis of an external *n*-alkane standard between samples yielded a root-mean-squared accuracy of 2‰ and a standard deviation of on average 3‰. The H_3-factor, used to correct for the formation of H_3^+ in the ion source, had a mean of 6.0 and varied between 5.8 and 6.2 throughout the analyses. Isotopic measurements were not made on samples Fran, Base of Frans, Fred, Frank, Fox, Fiona, Governor, Jack, Jude, Julia, Kate, Leo2 and Lynn due to low leaf-wax content.

5. Results

5.1 Bulk parameters

%TC is highly variable throughout the DRS sequence, ranging from ~2% to 37% (**Fig. 4a**). Major spikes in %TC are seen in SUs Frans, Fox, Fiona and Kenny. The high values of the bulk %TC are likely attributable to high contents of black carbon in the sediments, derived from combustion (Braadbaart et al., 2004; Braadbaart and Poole, 2008). However, %TC also incorporates organic carbon, which complicates the interpretation of %TC, but may explain its high variability. Bulk $\delta^{13}C_{TC}$ displays relatively little change, but tends to be lower during the SUs of the Late Howiesons Poort, averaging -24‰, compared to the SUs of the Early Howiesons Poort, which average -23‰ (**Fig. 4b**). %TN is high (up to 5%) and co-varies with %TC (**Fig. 4c**). Bulk $\delta^{15}N$ is very high, with values of > 20‰ throughout much of the record (**Fig. 4d**). Bulk $\delta^{15}N$ values are highest, but also most variable during the Late Howiesons Poort.

5.2 py-GC/MS

5.2.1 py-GC/MS in the absence of TMAH

The relative proportion of aliphatic compounds in the DRS sequence varies between 0 to 69% of the integrated ion current. The main contributors to this class are homologous sequences of *n*-alkane/*n*-alkene doublets spanning the chain length range C_8-C_{33} (**Fig. 5a,b**) Aliphatics are most prominent in samples LSA 1-3, and SUs Lynn, Logan, Keeno, Kerry, Joy, Jeff, John, Base of Eve, Ester and Eric (**Fig. 6**). The aliphatics include a high proportion of longer chain length *n*-alkanes, with an odd-over-even preference (**Fig. 5a,b**), which are most likely leaf-waxes that were not evaporated in the pyrolysis unit prior to analysis or bound to the sediment.

A distinct feature of several DRS pyrolysates (e.g. SUs Kim, Julia, Jack, Frank, Fred and Frans) is the presence of homologous sequences of alkyl-nitriles (up to C_{22} and peaking at C_{17} and C_{15} in most cases (**Fig. 5a,b**), with the exception of Leo 1), which make up 0-29% of the integrated ion current and are also of highest abundance in LSA 1-3, and SUs Lynn, Logan, Keeno, Kerry, Joy, Jeff, John, Base of Eve, Ester and Eric (**Fig. 6**).

Other nitrogen-containing compounds (i.e. excluding the alkyl-nitriles) include heterocyclic aromatic compounds, (methyl) pyrrole, acetonitrile, (methyl) pyridine, (methyl) indole, quinoline and (n-methyl) benzamide (**Fig. 5c**). The heterocyclic N-compounds are not typically diagnostic of particular source compounds but may be related to burning (Kaal and Rumpel, 2009). They make up 4-80% of the integrated ion current and are most abundant in Leo2, Leo1,

Kim, Julia, Jack, Governor, Fiona, Frank, Fred, Base of Frans, Frans and Eve (**Fig 6**).

Aromatic compounds contribute 10 to 48% of the total ion current (**Fig. 6**). They are dominated by benzene and to a lesser extent toluene and styrene (**Fig. 5c**). Typically they are not diagnostic of particular source compounds, although have been observed to increase in pyrolysates of materials associated with high charring temperatures (Kaal et al., 2009; Kaal and Rumpel, 2009; Kaal et al., 2012).

PAHs comprise up to 11% of the total ion current. Their abundance is particularly high in SUs Governor, Fiona, Frank, Fred, and Base of Frans (**Fig. 6**). The main contributors are naphthalene and small amounts of biphenyl, fluorene-9-one, n-methyl naphthalenes and anthracene (**Fig. 5c**).

Lignin monomers are found only in the LSA samples, contributing 9-17% of the total ion current. They are particularly well-preserved within LSA 1 (**Fig. 6**), where we observe an extensive array of products from coniferyl and syringyl lignin structures. Their absence in the MSA is likely due to degradation (Goñi and Hedges, 1992). Phenolic compounds are only present in a few samples, contribute up to 12% and are dominated by phenol. Their presence in the LSA samples may partly reflect their derivation from lignin monomers (Vane and Abbot 1999), or possibly proteins and tannins. Polysaccharides are present (2%–5%) only in the LSA and are absent in the MSA.

5.2.2 py-GC/MS in the presence of TMAH

The three samples analysed in the presence of TMAH (LSA 1, Logan and Ester) are dominated by C_{14}-C_{20} Fatty Acid Methyl Esters (FAMEs), peaking at C_{16} and C_{18}, with subordinate but variable contributions from long chain (C_{24}-C_{32}) FAMEs (**Fig. 5d-f**). The FAMEs are most likely derived from bound carboxylic (fatty) acid moieties and thus potentially a major source of the homologous alkane/alkene doublets in the non-treated pyrolysates. The FAMES may, however, also be partly derived from polymers, such as cutin (Del Rio and Hatcher 1998). The homologous alkyl nitriles are present but much less abundant in the TMAH analyses (**Fig. 5d-f**).

LSA 1 (**Fig. 5d**) produced multiple methylated lignin-related structures (e.g. the methyl ester of 3,4,5 trimethoxy benzoic acid (syringyl derivative), *m*-anisic acid methyl ester (4-methoxy benzoic acid methyl ester; *p*-coumaryl derivative) and 4-methy veratrole (3,4 dimethoxy toluene; guaiacyl derivative) consistent with the untreated analyses. The 3,4,5 methyl ester of trimethoxy benzoic acid may, however, also be tannin derived. Other features are the presence of *n*-methyl benzamide, hippuric acid methyl ester, tetramethyl uric acid (1,3,7,9-Tetramethyluric acid), and caffeine (1,3,7-Trimethylpurine-2,6-dione; structure strongly related to tetramethyl uric acid). These compounds are atypical of soils/Quaternary sediments within the study region (Carr et al 2014; unpublished data) and in the case of the hippuric acid methyl ester have only previously been reported, to our knowledge, in the pyrolysates of both rock hyrax midden material (Carr et al., 2010a) and amberrat, the resinous excretion of packrat urine (Fezzy and Armitage, 2006). Hippuric acid is a known

480 component of mammal urine (Bristow et al., 1992). Similarly, uric acid may be
481 derived from bird guano (Bird et al., 2008).

482 ### 5.3 Leaf-wax content and distribution

483 For the solvent-extracted leaf waxes, contents are highly variable; they exhibit a
484 maximum of 18.2 µg g^{-1} dw (for the C_{31} *n*-alkane; **Fig. 7**) but are below the
485 detection limit in SUs Jack, Governor, Fiona, Fox, Fred and Frans.
486
487 Leaf-wax $CPI_{25\text{-}33}$ ranges between 1.9 and 16.3 (average = 9.6; **Fig. 8**). Leaf-wax
488 $ACL_{14\text{-}35}$ ranges between 25.7 and 31.0 (average = 29.4) (**Fig. 8**). Through the
489 MSA, the ACL and CPI values display little overall trend, but SUs Leo2 and Debbie
490 display relatively low CPI, while SUs Leo2, Kate, Frank and Debbie display
491 relatively low ACL (**Fig. 8**).
492
493 The leaf-wax distribution of several SUs (e.g. Keeno) closely resembles the
494 average of modern Lowland Fynbos vegetation while other SUs (e.g. Eric)
495 resemble the average distribution of modern Succulent Karoo vegetation (**Fig.**
496 **3b**; Carr et al., 2014). For LSA 1- 3, Norm31 values range between 0.51 and 0.65
497 (**Fig. 9b**) and for the MSA values range between 0.54 and 0.83. For the SUs of the
498 Still Bay to Intermediate Howiesons Poort, values averaged 0.61 ± 0.05, while for
499 SUs of the Late Howiesons Poort values increase to, on average, 0.74 ± 0.05 (**Fig.**
500 **9b**).

501 ### 5.4 Leaf-wax isotopes

502 For samples LSA 1-3, $\delta^{13}C_{wax}$ for the C_{31} *n*-alkane (the most abundant and most
503 precisely measured homologue) ranges between -29.7‰ ± 0.2‰ and -30.4‰ ±

0.2‰. and (**Fig. 9a**). For the SUs of the MSA, values exhibit a relatively small range between -29.9‰ ± 0.1‰ and -31.8‰ ± 0.1‰. They are lowest in SUs Eve and Base of Eve (-31.8‰ ± 0.1‰), during the Late Howiesons Poort.

For samples LSA 1-3, δD_{wax} (**Fig. 9c**) ranges between -130‰ ± 1‰ and -147‰ ± 1‰. Through the MSA, δD_{wax} ranges between -140‰ ± 1‰ and -116‰ ± 1‰. Values are generally lower (mean = -133‰ ± 4‰) for the SUs of the Still Bay to Intermediate Howiesons Poort and higher (mean = -120‰ ± 4‰) for SUs of the Late Howiesons Poort.

6. Discussion

6.1 py-GC/MS: organic matter composition

py-GC/MS shows a clear organic matter compositional dichotomy. LSA 1-3, and SUs Lynn, Logan, Keeno, Kerry, Joy, Jeff, John, Base of Eve, Ester and Eric are rich in organic material and yield a range of pyrolysis products, most notably homologous sequences of *n*-alkane/*n*-alkene doublets and alkyl nitriles (**Fig. 5a,b**). Other samples (Leo2, Leo1, Kim, Julia, Jack, Governor, Fiona, Frank, Fred, Base of Frans, Frans and Eve) yield fewer pyrolysis products, and are dominated by aromatics and heterocyclic N (**Fig. 5c**). This major difference is inferred to reflect samples relatively rich in less-altered plant material, versus those that have undergone extensive burning or degradation.

Typical examples of SUs with a richer organic matter composition are John and Jeff, which exhibit the highest relative proportion of homologous alkane/alkene (aliphatic) pyrolysis products (**Fig. 6**). These are interpreted to be derived from

leaf cuticles, as revealed by the high abundance of long-chain FAMEs produced when the same samples are treated with TMAH (**Fig. 5d-f**), suggesting the presence of relatively fresh, unburnt plant derived organic matter (although note that more labile plant-derived OM such as lignin is not preserved in MSA SUs).

SUs exhibiting more burning include Leo 2, Kim, Julia, Jack, Governor, Fiona, Frank, Fred, Base of Frans, Frans and Eve (**Fig. 6**). These produce far higher proportions of aromatic, heterocyclic N, and PAH pyrolsysis products, with low abundances of aliphatics and leaf waxes. PAHs are particularly high for SUs Governor to Base of Frans (**Fig. 6**), and these likely reflect the most intensely heated samples (Kaal and Rumpel, 2009; Kaal et al., 2012). The pyrolysates show some commonalities with black carbon pyrolysates (Kaal et al., 2008), but are less diverse than pyrolysates of modern burned material (Kaal et al. 2009), likely due to degradation of the ancient MSA sediments. Based on laboratory burning experiments, a number of ratios (benzene/toluene, napthalene/C1-napthalene) have been proposed as indicators of burning intensity (Kaal and Rumpel, 2009; Kaal et al., 2012). The absence of toluene and C_1-napthalene in several SUs is likely due to incomplete preservation of these compounds. Nonetheless, several PAH, aromatic and heterocyclic-N pyrolysis products (Kaal and Rumpel 2009), are seen in the DRS pyrolysates (benzene, toluene, naphthalene, biphenyl, dibenzofuran and benzonitrile) and we take the summed integration of these as a summary indicator of black carbon and burning (**Fig. 10a**).

Although we often observe similarities in organic matter composition between adjacent SUs, we also note differences within individual SUs. For example, Eve

553 and Base of Eve, and Leo 1 and Leo 2 display a different organic matter
554 composition (**Fig. 6**). This highlights large differences in composition between
555 individual depositional units (microfacies units) within each SU (Miller et al.,
556 2013).
557
558 Another point of note is that LSA 2 is compositionally anomalous compared to
559 LSA 1 and LSA 3 in terms of the py-GC/MS analyses (**Fig. 6**), leaf-wax distribution
560 and isotopic analyses (**Fig. 9**). This might reflect some admixing of the MSA
561 material into the LSA, which would account for the absence of lignin and
562 cellulose pyrolysis products in LSA 2, despite their conspicuous presence in LSA
563 1 and LSA 3.

564 ## 6.2 Nitrogen containing compounds

565 Notable in the py-GC/MS data are the relatively high abundances of the nitrogen-
566 containing compounds in some samples, notably the homologous sequences of
567 alkyl nitriles. These are not observed in natural soils in the region, and the TN
568 content of the DRS sediments (**Fig. 4c**), is also substantially higher than modern
569 soils (Carr et al., 2013). The alkyl nitriles as pyrolysis products were previously
570 observed to form from the fragmentation of aliphatic molecules (probably the
571 C_{18} fatty acid; **Fig 5e,f**) during pyrolysis in the presence of ammonia and clay
572 (Nierop and van Bergen, 2002). The source of ammonia in this context may be
573 related to the hippuric acid and uric acid pyrolysis products identified in the LSA
574 py-GC/MS data. The latter is known to degrade to ammonia, explaining its
575 absence in the MSA pyrolysates (Mizutani and Wada, 1985), while
576 micromorphological analyses have previously identified a thick niter crust at the

577 top of the sediments (Miller et al., 2013). Rock hyraxes were identified as a likely
578 N source in the sediments (Miller et al., 2013) and the presence of benzamide,
579 uric acid/hippuric acid (methylated forms) in the LSA pyrolysates is consistent
580 with the composition of hyraceum, strongly pointing to urine contributions in
581 two of the LSA samples (Carr et al., 2010a; Fezzy and Armitage, 2006). Guano,
582 however, might be an additional source of N (Miller et al., 2013) and of the very
583 high bulk $\delta^{15}N$ values of the DRS sediment (19-32‰; **Fig. 4d**), which are
584 significantly higher than local vegetation (typically -4 to 5‰ (Sealy et al., 1987;
585 Stock et al., 1995), soils (typically 7-10‰ in the Lowland Fynbos; Carr et al.,
586 unpublished data), and hyraceum (typically 5-10‰; (Carr et al., 2016a). The
587 impact of guano on soil $\delta^{15}N$ has been reported previously, with guano-fertilised
588 plant $\delta^{15}N$ experimentally enhanced by up to 20‰ relative to a control (Szpak et
589 al., 2012), a magnitude consistent with the difference between DRS sediments
590 and local plants/soils. Degradation of such N inputs to ammonia in the older MSA
591 materials is therefore a plausible source of N for the production of the alkyl
592 nitriles during pyrolysis.

593 ### 6.3 Leaf-wax content and distribution as burning indicators

594 The content of extracted leaf waxes from the LSA samples (2.7 - 9.0 ug g^{-1} dw)
595 and MSA samples (0 - 18.2 µg g^{-1} dw; for the C_{31} *n*-alkane) are similar to
596 contemporary Lowland Fynbos soils (0.4 - 5.6 µg g^{-1} dw; Herrmann et al., 2016).
597 The high content of leaf waxes in many SUs (Logan, Keeno, Joy, John, Ester, Eric;
598 **Fig. 7**) is in line with the input of grasses to the shelter (Cartwright, 2013; Miller
599 et al., 2013), presumably used for bedding, and supports the py-GC/MS evidence
600 for leaf cuticle input in SUs John and Jeff. The high leaf-wax content attests to

601 excellent preservation potential of these compounds within DRS, presumably
602 due either to the aridity of the shelter, or possibly to the high proportion of black
603 carbon, which may have inhibited degradation (Hernandez‐Soriano et al.,
604 2016). The high content of leaf waxes also argues against extensive heating of
605 these SUs.
606
607 In contrast, however, the absence of leaf-wax *n*-alkanes in SUs Jack, Governor,
608 Fiona, Fox, Fred and Frans (**Fig. 7**) is in line with more intensive burning or
609 heating of these samples, as also inferred from the py-GC/MS: the pyrolysis
610 products from these SUs being dominated by aromatics and PAHs (**Fig. 6**).
611
612 Although waxes are present in SUs Leo2, Kate, Frank and Debbie, these SUs
613 exhibit lower CPIs (1.9 to 5.9) and lower ACLs (25.7 to 27.6) compared to the
614 unburnt straw and soils, which likely reflects moderate heating (**Fig. 8**). The ACL
615 values of these samples are close to those of the 300°C burning experiments of
616 Wiesenberg et al., (2009), possibly indicating heating of these samples to similar
617 temperatures (**Fig. 8**). The pyrolysates of Leo 2 and Frank are also dominated by
618 heterocyclic N products and PAHs (**Fig. 6**). Although there are differences in
619 character of the vegetation brought into DRS and the rye and maize used in the
620 laboratory burns, these temperature estimates are not inconsistent with
621 maximum temperatures measured beneath experimental fires using South
622 African vegetation (~300 °C; Sievers and Wadley, 2008). We do not observe the
623 increase in mid- and short-chain *n*-alkanes (Wiesenberg et al., 2009), although
624 this may reflect post-depositional degradation of these homologues (Cranwell,
625 1981).

626

627 Aside from SUs Leo2, Kate, Frank and Debbie, the remaining DRS MSA samples
628 exhibit ACL values (28.8 to 31.0) within the range of the unburnt straw samples
629 (29.6 to 30.2) and the Succulent Karoo (30.0 ± 1.0) and Lowland Fynbos (28.8 ±
630 0.7) soils (**Fig. 8**; Carr et al., 2014). The CPI values of these DRS MSA samples are
631 in some cases lower than soils and unburnt straw (**Fig. 8**), although given the
632 high ACL values, this may reflect the samples age rather than extensive heating.
633 Given that charcoal (Miller et al., 2013) and PAHs (**Fig. 6**) are present in these
634 SUs, it seems likely that they represent a mixture of both unheated and
635 heated/burnt plant material.

636

637 Overall, our leaf wax data suggests that 1) some SUs (i.e. those lacking leaf
638 waxes) were extensively heated/burnt; 2) other SUs (i.e. those with low ACL)
639 were heated to 300°C or less; and 3) most SUs (i.e. those with ACL similar to
640 unburnt straw) were heated very little. Perhaps those of type 1 represent direct
641 sampling of ashes or hearths, those of type 2 represent material that was
642 positioned underneath active hearths, and type 3 represents unheated or only
643 slightly heated material. In general, SUs without *n*-alkanes generally show high
644 proportions of PAHs, heterocyclic N and aromatics in their pyrolysates, while
645 those with high *n*-alkane abundances show lower PAH, heterocyclic N and
646 aromatics (**Fig. 10a,b**), indicating a clear relation to heating.

647 ### 6.4 Organic markers compared to micromorphology

648 Micromorphological analyses (Miller et al., 2013) identified SUs John and Jeff
649 (Lithostratigraphic Unit 3; **Fig. 10**) as containing a higher proportion of humified

material relative to combustion features compared with other MSA SUs. Our data suggest high abundances of aliphatics, high leaf-wax content and low abundances of PAHs for these SUs, in line with the micromorphological findings (**Fig. 10a,b**).

In contrast, SUs Governor to Debbie (Lithostratigraphic Unit 4) contain a significantly higher proportion of charcoal and evidence for raking out of hearths and the removal of unburnt material (Miller et al., 2013). This agrees with the increased py-GC/MS indicators for black carbon (**Fig. 10a**) and decreased leaf-wax content (**Fig. 10b**). Moreover, SU Fred was reported to contain burnt bedding (Miller et al., 2013) and here we observe the highest PAH proportion of the whole dataset and high heterocyclic N content (**Fig. 6**). Overall, our findings are therefore complementary to those of the micromorphology.

Changes in burning and site use intensity might be expected to go hand in hand with indicators of human behavioural changes, such as engraved ostrich eggshell (EOES; Texier et al., 2013). The earliest evidence for EOES at DRS is between SUs Julia to Jack, which display evidence for extensive burning (**Fig. 10a-c**). Similarly, going up the sequence, EOES content begins to increase at SU Governor and remains high for much of Lithostratigraphic Unit 4, when we observe a high degree of burning (**Fig. 10a-c**). Thus, our burning data provide support for changes in site usage.

6.5 Vegetation-type inferences from Norm31

Norm31 for the LSA (0.56 ± 0.08) is highly comparable to modern Lowland Fynbos soils close to DRS (0.57 ± 0.20; **Fig. 9b**). Although we note the large range

674 in values of modern vegetation, this similarity would support the use of Norm31
675 as past vegetation indicator.
676
677 Between the Still Bay and Intermediate Howiesons Poort, Norm31 averaged 0.60
678 ± 0.05, while during the Late Howiesons Poort it increased to 0.74 ± 0.05 (**Fig.**
679 **9b**). This Norm31 increase implies more arid-adapted vegetation was being
680 brought into the shelter during the Late Howiesons Poort. This might reflect a
681 change in the collecting habits of the inhabitants (towards more arid adapted
682 vegetation) or a change in the climate conditions/ecology around the shelter
683 towards those resembling the modern Succulent Karoo biome, such as increased
684 summer aridity. Either way, a shift in the vegetation brought into the site
685 appears to be in line with findings from charcoal remains, which suggest a shift
686 to more dry-adapted thicket vegetation during the Howiesons Poort (Cartwright,
687 2013). It should be noted that the Late, Intermediate and Early Howiesons Poort
688 were not differentiated in the charcoal study, and it is implied that the
689 aridification began during the Early Howiesons Poort. Nonetheless, the author
690 notes that the post-Howiesons Poort shows a continuing trend towards arid-
691 tolerant thicket and shrubland.

692 ### 6.6 $\delta^{13}C_{wax}$ and vegetation

693 The mean $\delta^{13}C_{wax}$ for the LSA (-29.8‰ ± 0.4‰; **Fig. 9a**) is slightly higher than
694 soil samples from the Lowland Fynbos close to DRS (-32.3‰ ± 2‰; Herrmann
695 et al., 2016; **Fig. 9a**). This might reflect the selection of certain plants by the
696 inhabitants, perhaps for use as bedding or food. These values lie in between
697 those of C_3 vegetation (mean of -34.2‰ ± 4‰), and CAM (-22.7‰ ± 6‰; Boom

et al., 2014) and C_4 vegetation (-21.8‰ ± 2‰; Rommerskirchen et al, 2006), thus likely reflect a mixture of several vegetation types.

Throughout the MSA, $\delta^{13}C_{wax}$ values exhibit little variation, varying between -29.9‰ ± 0.1‰ and -31.8‰ ± 0.1‰ (**Fig. 9a**). The bulk $\delta^{13}C_{TC}$ also displays limited change, of the order of 1‰ (**Fig. 4b**). Limited vegetation change is implied, in line with the stability of the Fynbos biome inferred elsewhere (Dupont et al., 2011). In light of the large range of values exhibited in the modern soils (Herrmann et al., 2016) and plant samples (Boom et al., 2014), the small variability in DRS may reflect averaging over the wide range of taxa that were brought into the site through the MSA, evident in the charcoal assemblage (Cartwright, 2013). Furthermore, from the $\delta^{13}C_{wax}$ stability, we can rule out dominant input of the C_4 halophytic grasses into the shelter (*Spartina maritima*) that today grow on the margins of the Verlorenvlei Estuary, or of CAM plants that might be used as food (e.g. fruits of *Carpobrotus edulis*) or as kindling (e.g. large stems of plants such as *Ruschia*).

6.7 δD_{wax} and hydroclimate

The LSA mean δD_{wax} value of -141‰ ± 10‰ is in line with the contemporary soil samples from the DRS locale (mean of -143‰ ± 9‰; Herrmann et al., 2017), suggesting that sedimentary δD_{wax} is representative of the mean δD_{wax} of vegetation from the region surrounding the shelter.

Moreover, throughout the MSA and LSA, δD_{wax} and $\delta^{13}C_{wax}$ values are within the range of modern plants from the wider region (**Fig. 1b; 9c**). This suggests that

722 burning probably has a minor effect on δD_{wax} and $\delta^{13}C_{wax}$. It seems that while
723 severely burnt SUs (e.g. Governor, Fred, Frans) are devoid of leaf waxes, slightly
724 heated SUs (e.g. Debbie) show comparable δD_{wax} values to adjacent unheated SUs
725 (**Fig. 9a,c**).
726
727 Modern soil samples display an increase in *n*-alkane δD_{wax} to the NE of DRS (i.e.
728 into the Succulent Karoo; **Fig. 1b**). This was interpreted (Herrmann et al., 2017)
729 to reflect: a) an increase in δD_p from SW to NE due to decreasing precipitation
730 amount, and b) a decrease in relative humidity from SW to NE, inducing
731 increased evapotranspirational isotopic enrichment of leaf and soil water. There
732 may be an additional secondary effect on δD_{wax} associated with c) different
733 hydrogen isotope fractionation of different plant types, with C_3 trees and shrubs
734 and CAM plants tending to yield higher values than C_3 grasses (Feakins and
735 Sessions, 2010; Sachse et al., 2012).
736
737 Between the Still Bay and Intermediate Howiesons Poort, δD_{wax} was slightly
738 higher than the present (average -133‰ ± 4‰), while during the Late
739 Howiesons Poort (SUs Eve to Debbie) δD_{wax} increased further (average -120‰ ±
740 4‰; **Fig. 9c**). The Late Howiesons Poort increase likely represents input of
741 vegetation that has been subject to a) less precipitation or b) more
742 evapotranspiration (more intense summer drought), and/or may reflect c) input
743 of more shrub-like vegetation rather than grasses.
744
745 Input of more shrub-like vegetation during the Late Howiesons Poort would be
746 consistent with the inference of a shift to arid-adapted vegetation during the Late

747 Howiesons Poort from the Norm31 (**Fig. 9b**) and might be reflecting a shift in the
748 inhabitants' vegetation selection strategy. A change in inhabitants' vegetation
749 selection strategy during the Late Howiesons Poort would seem plausible given
750 the other evidence for behavioural changes including the increased EOES (above
751 Governor) and increased burning (Governor to Frans; **Fig. 10**). Leaf-wax content
752 was, however, too low for analysis between Governor and Frans and so we
753 cannot be certain that the δD_{wax} changes were coeval with the site usage changes.
754
755 Alternatively, the δD_{wax} variability may be reflecting hydroclimate changes. The
756 above scenarios a, b and c would all broadly represent increased aridity during
757 the Late Howiesons Poort. In support of hydroclimate rather than selection
758 strategy as the control on δD_{wax}, we note that the global climate of MIS5 was
759 more similar to MIS1 than to MIS3/4, in terms of ice volume and temperature.
760 Based on the Tribolo et al., (2013) chronology, the δD_{wax} and Norm31 both
761 suggest that MIS5 (130-71ka) and MIS1 (10-0ka) were less arid, while MIS4 (71-
762 57ka) and MIS3 (57-29ka), corresponding to the Late Howiesons Poort, were
763 more arid (**Fig. 9b,c**). Nonetheless, we note that this reasoning relies on a
764 chronology that at present is controversial.

765 ## 7. Conclusions

766 We investigated the potential of organic matter preserved in the MSA sediments
767 of Diepkloof Rock Shelter to understand site usage and past climate. Py-GC/MS
768 revealed that while some samples contain a high abundance of relatively un-
769 altered plant material, others were low in organic matter and are composed
770 largely of aromatic, heterocyclic N and PAH pyrolysis products, indicative of

771 higher burning intensity. The highest degree of burning is between SUs Governor
772 and Frans, in line with micromorphological findings for increased charcoal
773 content. By contrast, SUs John and Jeff display a higher abundance of humified
774 organic matter. The high N content of the sediment is interpreted as reflecting
775 inputs of hyrax urine/hyraceum and/or contributions from bird guano,
776 consistent with the high bulk $\delta^{15}N$ values.
777
778 We found variable but often high contents of leaf waxes. Most samples display
779 leaf-wax *n*-alkane distributions typical of modern plants in the region, suggesting
780 heating temperatures < 300°C. This is consistent with the correspondence
781 between $\delta^{13}C_{wax}$ and δD_{wax} from DRS and modern soils in the region. SUs from
782 the Late Howiesons Poort display longer *n*-alkane chain-length distributions and
783 increased δD_{wax} values compared to the Still Bay, Intermediate Howiesons Poort
784 and the LSA. This likely represents a shift towards input of more arid-adapted
785 vegetation during the Late Howiesons Poort, reflecting aridification, or a change
786 in selection strategy of the inhabitants. Overall, these results underline the
787 potential of these organic-geochemical methods to support and augment
788 interpretations of site usage and environmental context of rock shelter
789 occupations.

790 ## Figure captions

791

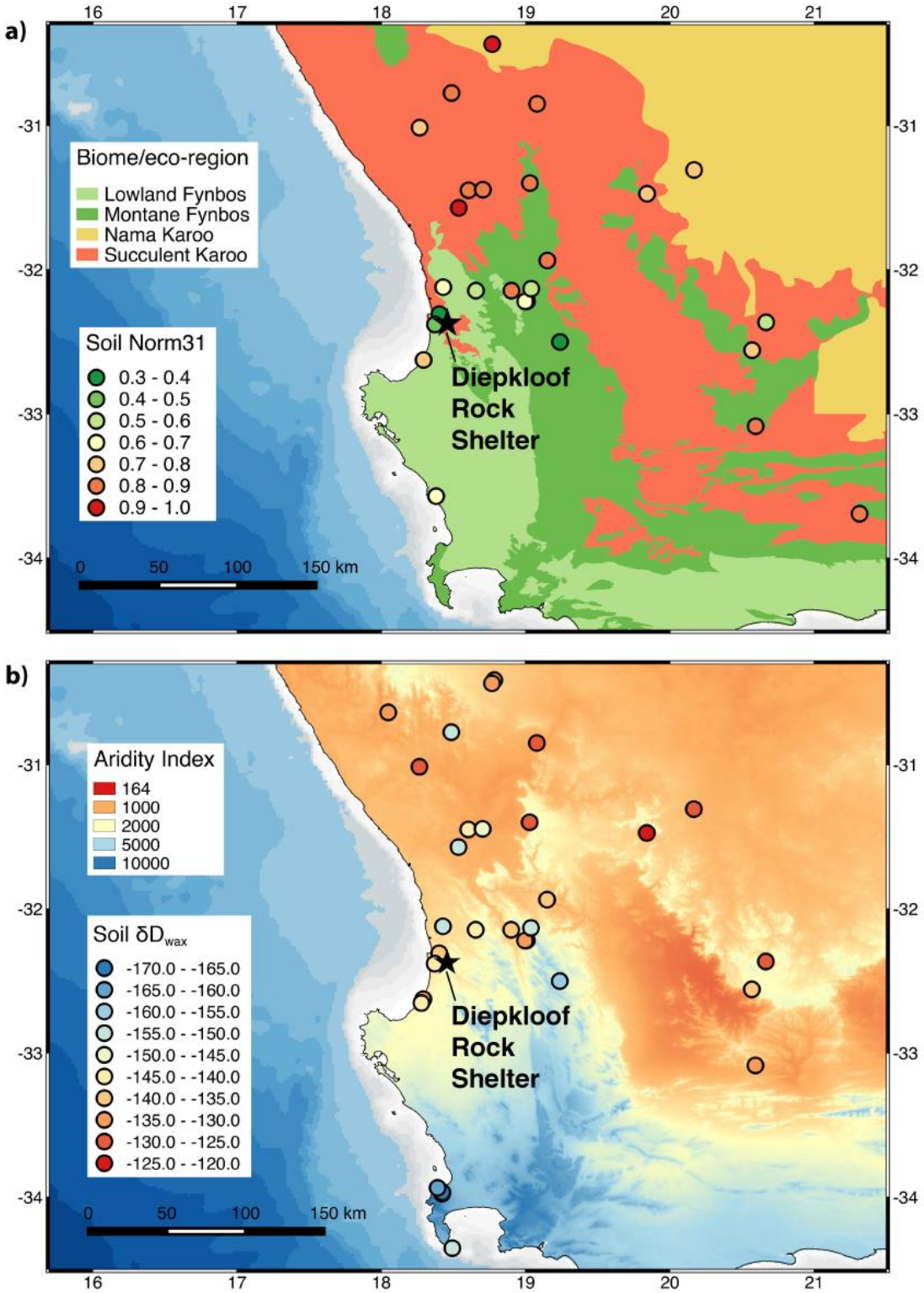

Fig. 1. Maps of biomes/eco-regions and aridity. a) Biomes and eco-regions in southwestern Africa (Rutherford et al., 2006). Circles indicate the Norm31 of *n*-alkanes from contemporary soils (Carr et al., 2014). **b)** Aridity index (Trabucco and Zomer, 2009), calculated as mean annual precipitation / mean annual

potential evapotranspiration, where higher values represent less arid conditions. Circles indicate the δD_{wax} of the C_{31} *n*-alkane from contemporary soils (Herrmann et al., 2017). Bathymetry shaded grey is 0-120m depth with contours every 20m.

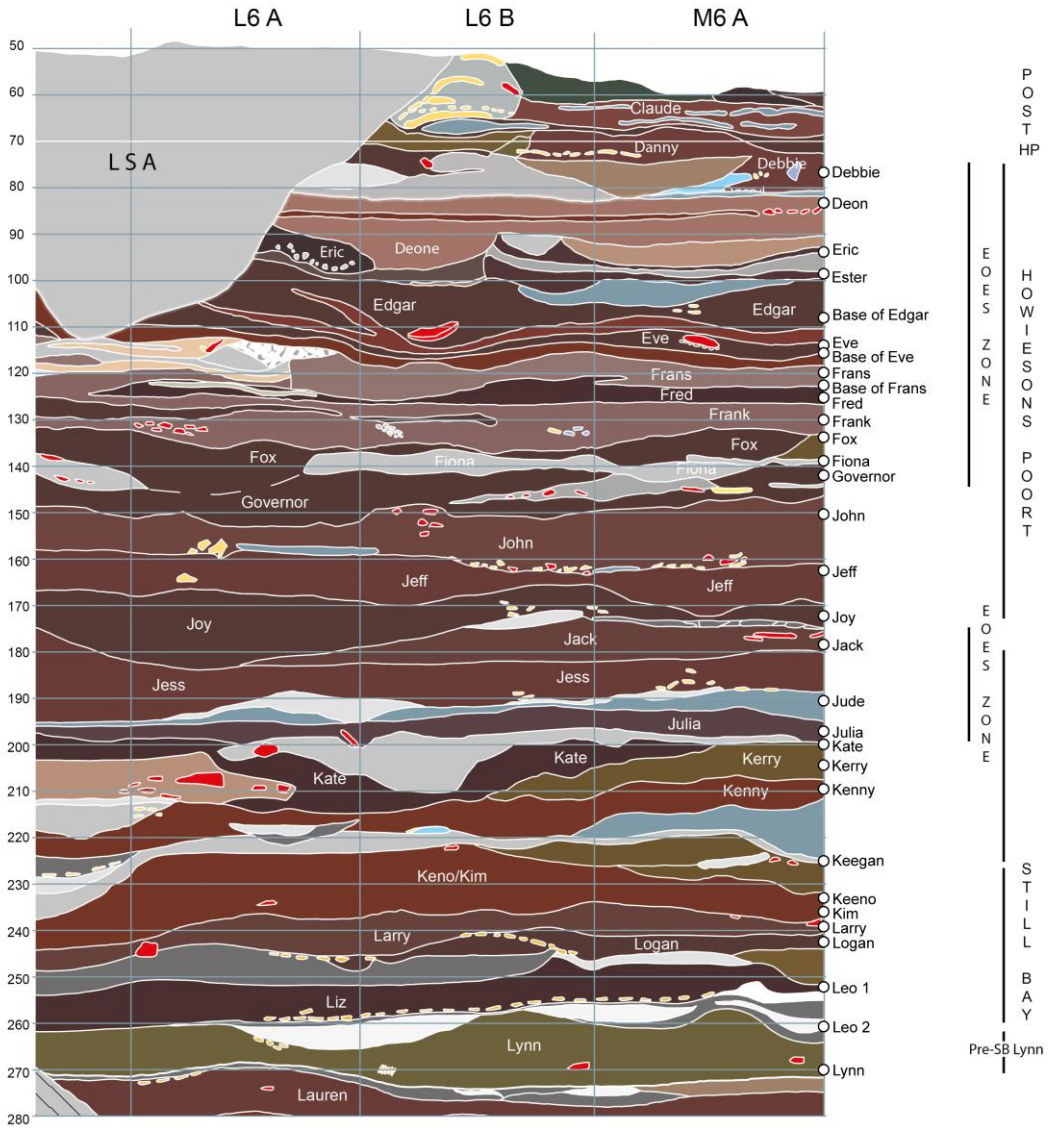

Fig. 2. Diepkloof Rock Shelter section. Shown are the stratigraphic units (SUs), technocultural subdivisions and the zone of high abundance of engraved ostrich eggshell (EOES). MSA samples analyzed in this study were taken from square M7 and are marked as white circles on the right hand edge of the figure (figure modified from Texier et al., 2013).

807

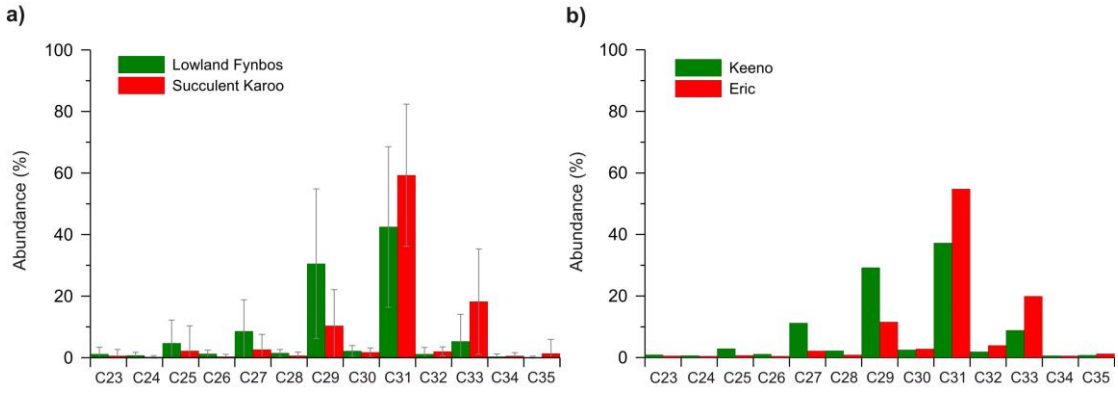

808

809 **Fig. 3. Comparison of *n*-alkane distribution in locally sourced plants and**

810 **Diepkloof Rock Shelter sediments. a)** Lowland Fynbos (n= 28) and Succulent

811 Karoo (n=133; Carr et al., 2014) plants. **b)** SU Keeno displays a Fynbos-like

812 distribution (dominance of C_{31} and C_{29}), while SU Eric displays a Succulent

813 Karoo-like distribution (dominance of C_{31} and C_{33}).

814

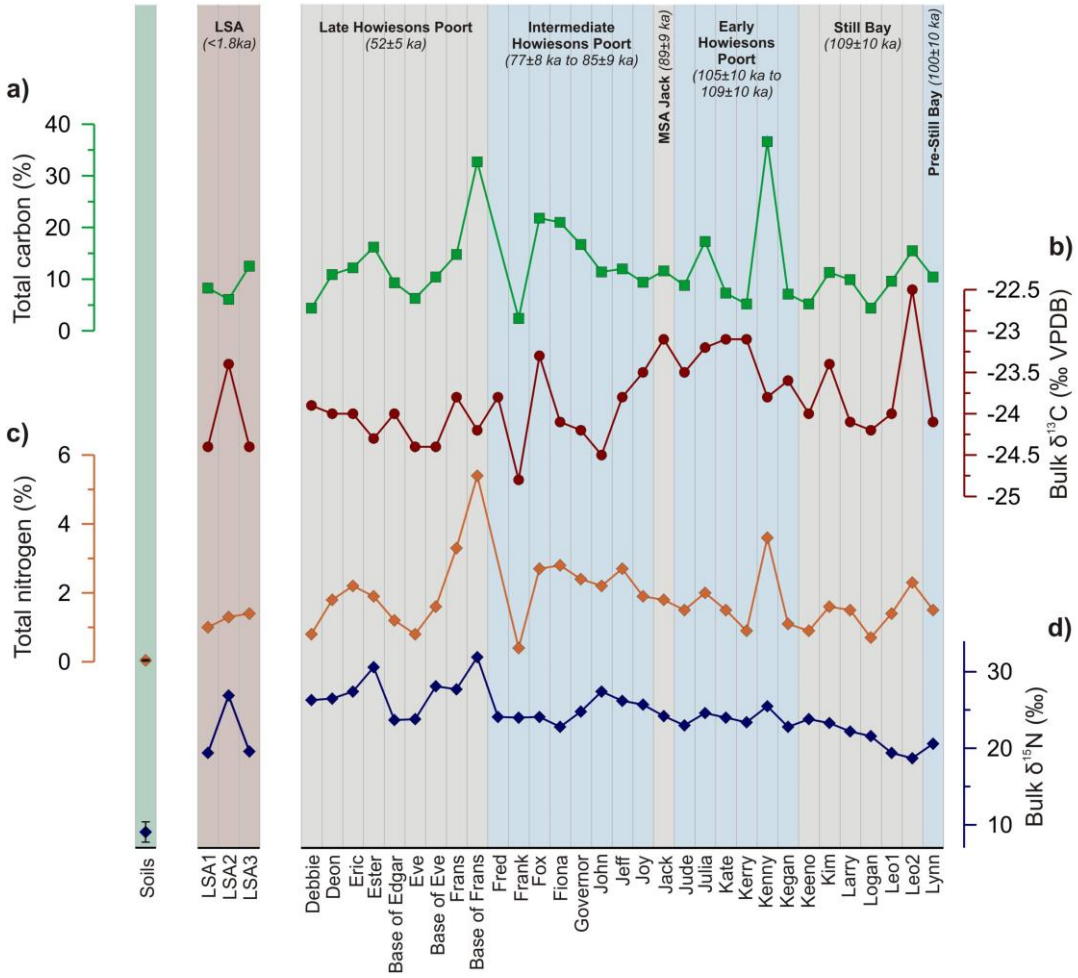

815

816 **Fig. 4. Bulk parameters for the LSA and MSA sediments. a)** Total carbon
817 (%TC), **b)** Bulk $\delta^{13}C_{TC}$ (‰ VPDB), **c)** Total nitrogen (%TN) **d)** Bulk $\delta^{15}N$ (‰).
818 Values of %TN and bulk $\delta^{15}N$ from modern Lowland Fynbos soils close to DRS
819 are shown (values are mean of samples SV2-SV5 which are located within about
820 30km of DRS; n=14; errors bars are one sigma; Carr et al. 2013 and unpublished
821 data). Technocultural subdivisions are marked above, along with the estimated
822 ages (Tribolo et al., 2013).

823

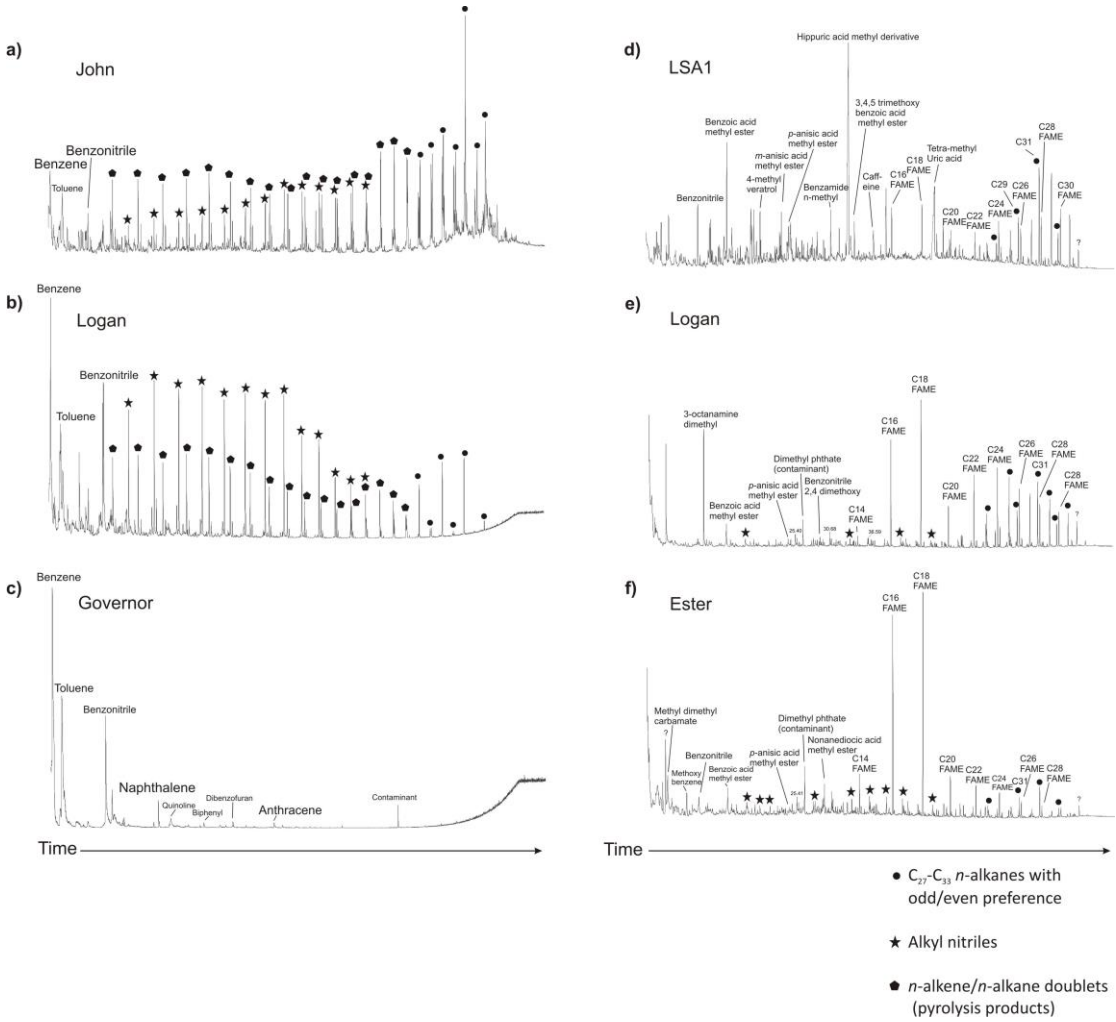

Fig. 5. Pyrograms for selected samples showing the range of compounds identified by py-GC/MS. a)-c) Selected samples run in the absence of TMAH, **d)-f)** Selected samples run in the presence of TMAH.

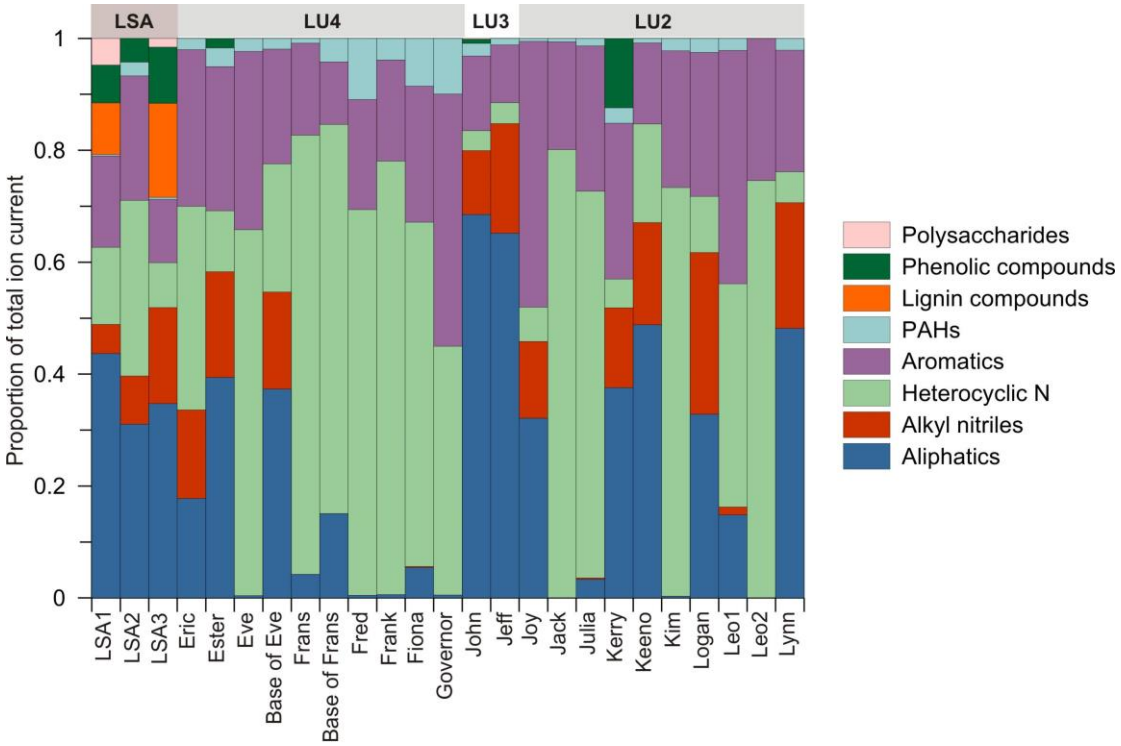

828

829 **Fig. 6. Relative proportion of compound classes in MSA ad LSA sediments**

830 **derived from py-GC/MS analyses.** Shown are measurements made in the

831 absence of TMAH. Lithostratigraphic Units (LUs) as defined in Miller et al.,

832 (2013) are given above.

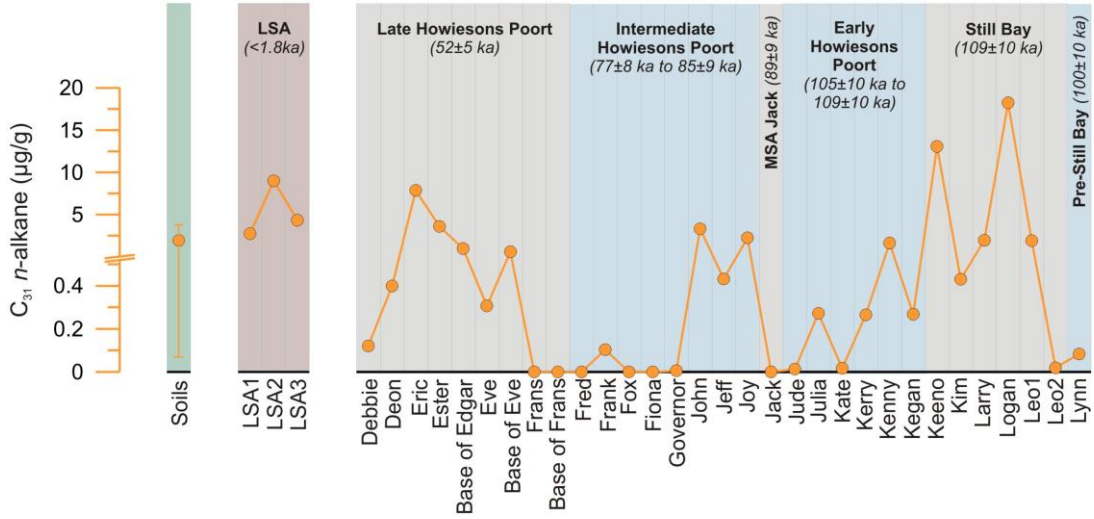

833

834 **Fig. 7. Leaf-wax *n*-alkane content from LSA and MSA sediments.** C_{31} *n*-alkane

835 content (µg g dw^{-1}). Technocultural subdivisions are marked above (Porraz et al.,

836 2013) along with their age ranges (Tribolo et al., 2013). C_{31} *n*-alkane content for

modern Lowland Fynbos soils is shown (values are mean of samples SV2-SV5, which are located within about 30km of DRS; n=6; error bars are one sigma; Carr et al., 2014; Herrmann et al., 2016).

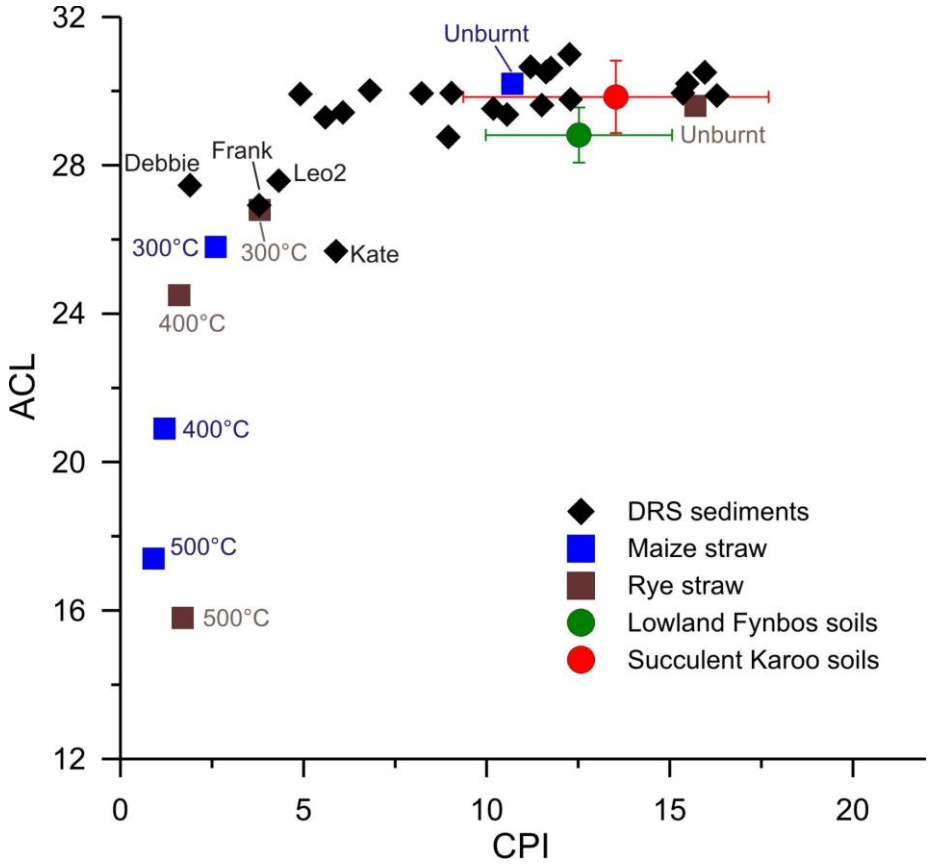

Fig. 8. $CPI_{25\text{-}33}$ and $ACL_{14\text{-}35}$ from DRS sediments, laboratory burned straw and soils from the region. Black diamonds represent MSA sediments from DRS; blue and brown squares represent values at different temperatures from the burning experiments of maize and rye straw (Wiesenberg et al., 2009). Green and red circles represent mean values from the full dataset of Lowland Fynbos (n=15; error bars one sigma) and Succulent Karoo (n=53) soils (Carr et al., 2014). For the straw, $CPI_{27\text{-}33}$ is shown.

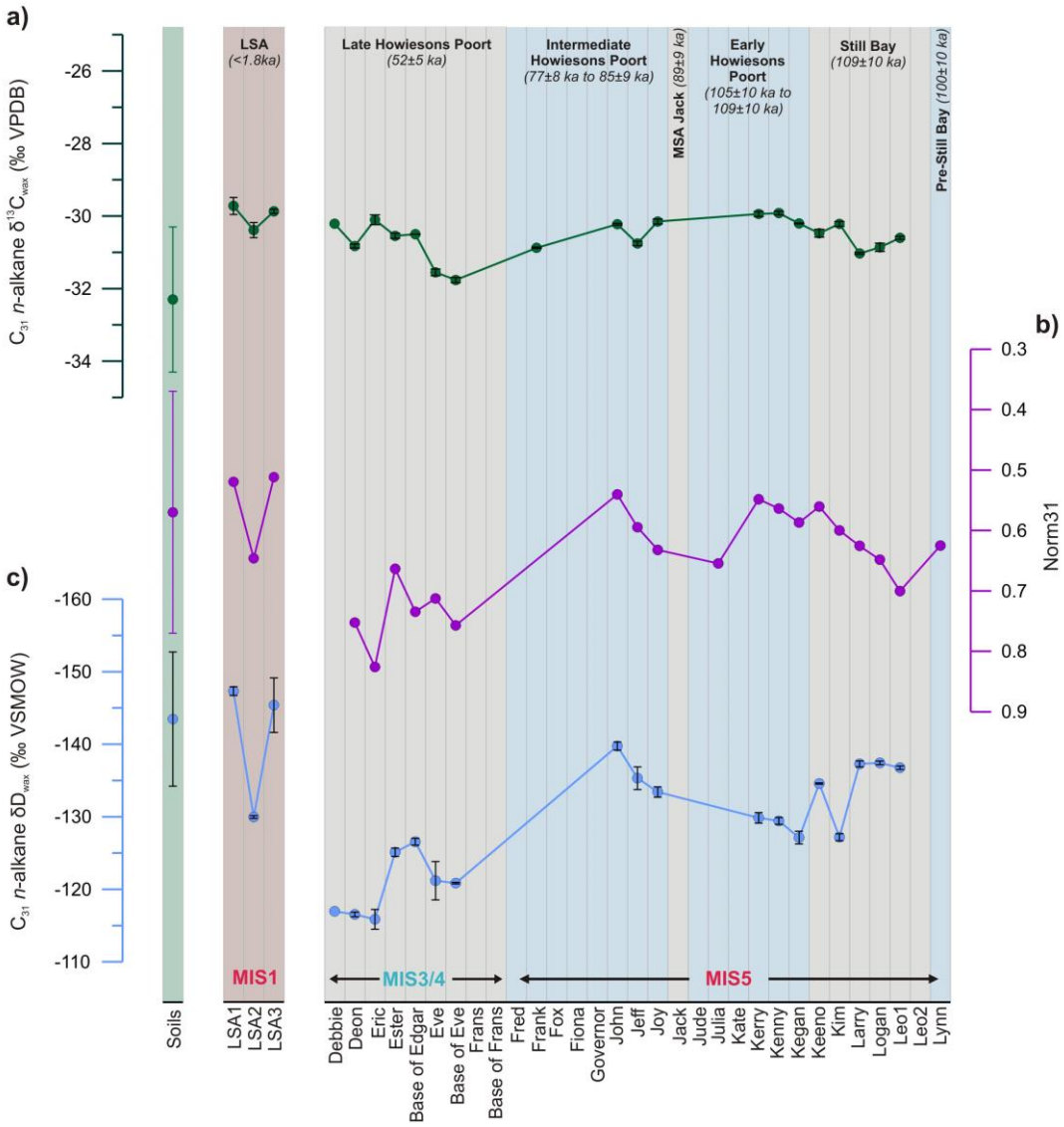

Fig. 9. Vegetation and hydroclimate indicators from Diepkloof Rock Shelter sediments. a) C_{31} *n*-alkane $\delta^{13}C_{wax}$. Error bars represent one sigma measurement precision. **b)** Norm31, (excluding samples Debbie, Frank, Kate, Leo2, which show evidence of heating). **c)** C_{31} *n*-alkane δD_{wax}. Error bars represent one sigma measurement precision. $\delta^{13}C_{wax}$, Norm31 and δD_{wax} values for modern soil samples are shown (mean of samples SV2-SV5, located within about 30km of DRS; n=6; error bars are one sigma; Herrmann et al., 2016, 2017). Marine Isotope Stages (MIS) into which the SUs would fall (based on the age model of Tribolo et al., 2013) are marked.

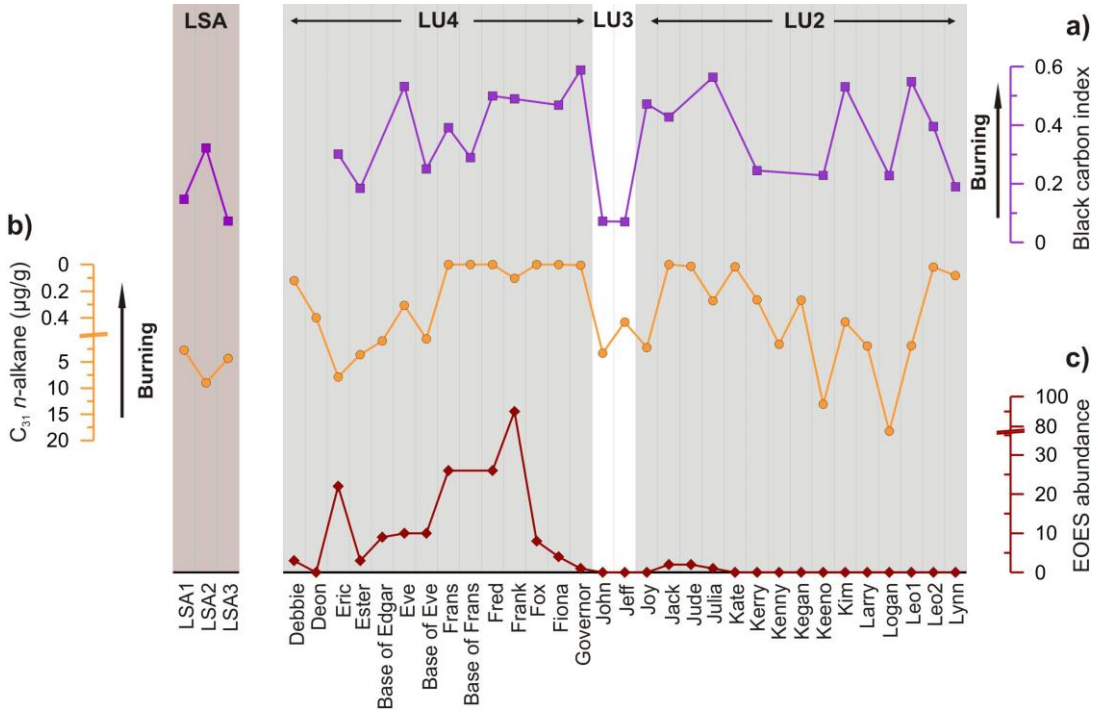

858

859 **Fig. 10. Summary of burning indicators and EOES. a)** Black carbon index,
860 which is the sum of the relative proportion of benzene, toluene, naphthalene,
861 biphenyl, dibenzofuran and benzonitrile (Kaal and Rumpel, 2009). **b)** C_{31} *n*-
862 alkane content (note inverted axis), **c)** Number of engraved ostrich eggshells
863 (EOES) within each SU (Texier et al., 2013). Lithostratigraphic Units (LUs) 2-4
864 are marked (Miller et al., 2013).

Acknowledgements

Excavations at Diepkloof were funded by the French Ministry of Foreign Affairs (MAE), the Aquitaine region, the Provence-Alpes-Côte-d'Azur region, the Centre National de la Recherche Scientifique (CNRS) as well as by the Palaeontological Scientific Trust (PAST) and the National Research Foundation (NRF) of South Africa. D. & M. van Wyk and J. Pollet gave permission for the excavations to take place. We thank Guillaume Porraz and Pierre-Jean Texier for allowing us to take sediment samples, and facilitating this process in the field. Christopher Miller provided invaluable help during sampling. Ian Newton, Nicoletta Ruggieri and Ralph Kreutz are thanked for their assistance in the lab. Thanks to Pierre-Jean Texier for providing the stratigraphic section in Figure 2, and Matthew Lewis for assistance with modifying it. Emma Pearson is thanked for providing additional soil samples from South Africa. Data from those samples have been generated by Katharina Siedenberg. James A. Collins was funded by the Helmholtz Postdoc Programme (PD-001) and the Alfred Wegener Institute for Polar and Marine Research, Bremerhaven. Judith Sealy acknowledges support from the South African Research Chairs initiative of the Department of Science and Technology and National Research Foundation of South Africa. The compound-specific isotope analyses were supported by the DFG-Research Center / Cluster of Excellence „The Ocean in the Earth System" at MARUM - Center for Marine Environmental Sciences.

Conflicts of interest

The authors declare that they have no conflict of interest.

References

Ballentine, D.C., Macko, S.A., Turekian, V.C., 1998. Variability of stable carbon isotopic compositions in individual fatty acids from combustion of C4 and C3 plants: implications for biomass burning. Chem. Geol. 152, 151-161.

Bird, M.I., Tait, E., Wurster, C.M., Furness, R.W., 2008. Stable carbon and nitrogen isotope analysis of avian uric acid. Rapid Commun. Mass Spectrom. 22, 3393-3400.

Boom, A., Carr, A., Chase, B., Grimes, H., Meadows, M., 2014. Leaf wax n-alkanes and δ13C values of CAM plants from arid southwest Africa. Org. Geochem. 67, 99-102.

Braadbaart, F., Boon, J.J., Veld, H., David, P., van Bergen, P.F., 2004. Laboratory simulations of the transformation of peas as a result of heat treatment: changes of the physical and chemical properties. Journal of Archaeological Science 31, 821-833.

Braadbaart, F., Poole, I., 2008. Morphological, chemical and physical changes during charcoalification of wood and its relevance to archaeological contexts. Journal of archaeological science 35, 2434-2445.

Carr, A.S., Boom, A., Chase, B.M., 2010a. The potential of plant biomarker evidence derived from rock hyrax middens as an indicator of palaeoenvironmental change. Palaeogeogr. Palaeoclimatol. Palaeoecol. 285, 321-330.

Carr, A.S., Boom, A., Chase, B.M., Meadows, M.E., Roberts, Z.E., Britton, M.N., Cumming, A.M., 2013. Biome-scale characterisation and differentiation of

913 semi-arid and arid zone soil organic matter compositions using pyrolysis–GC/MS
914 analysis. Geoderma 200, 189-201.
915 Carr, A.S., Boom, A., Chase, B.M., Roberts, D.L., Roberts, Z.E., 2010b.
916 Molecular fingerprinting of wetland organic matter using pyrolysis-GC/MS: an
917 example from the southern Cape coastline of South Africa. J. Paleolimnol. 44,
918 947-961.
919 Carr, A.S., Boom, A., Grimes, H.L., Chase, B.M., Meadows, M.E., Harris, A.,
920 2014. Leaf wax n-alkane distributions in arid zone South African flora:
921 environmental controls, chemotaxonomy and palaeoecological implications. Org.
922 Geochem. 67, 72-84.
923 Carr, A.S., Chase, B.M., Boom, A., Medina-Sanchez, J., 2016a. Stable isotope
924 analyses of rock hyrax faecal pellets, hyraceum and associated vegetation in
925 southern Africa: Implications for dietary ecology and palaeoenvironmental
926 reconstructions. Journal of Arid Environments 134, 33-48.
927 Carr, A.S., Chase, B.M., Mackay, A., 2016b. Mid to Late Quaternary
928 landscape and environmental dynamics in the Middle Stone Age of southern
929 South Africa, Africa from MIS 6-2. Springer, pp. 23-47.
930 Cartwright, C.R., 2013. Identifying the woody resources of Diepkloof Rock
931 Shelter (South Africa) using scanning electron microscopy of the MSA wood
932 charcoal assemblages. Journal of Archaeological Science 40, 3463-3474.
933 Challinor, J.M., 2001. Review: the development and applications of
934 thermally assisted hydrolysis and methylation reactions. J. Anal. Appl. Pyrolysis
935 61, 3-34.
936 Charrié-Duhaut, A., Porraz, G., Cartwright, C.R., Igreja, M., Connan, J.,
937 Poggenpoel, C., Texier, P.-J., 2013. First molecular identification of a hafting

938 adhesive in the late Howiesons Poort at Diepkloof Rock Shelter (Western Cape,
939 South Africa). Journal of Archaeological Science 40, 3506-3518.
940 Chase, B.M., 2010. South African palaeoenvironments during marine
941 oxygen isotope stage 4: a context for the Howiesons Poort and Still Bay
942 industries. Journal of Archaeological Science 37, 1359-1366.
943 Cowling, R.M., Richardson, D.M., Mustart, P.J., 1997. Fynbos, in: Cowling,
944 R.W., Richardson, D.M., Pierce, S.M. (Eds.), Vegetation of Southern Africa.
945 Cambridge University Press, Cambridge, pp. 99–130.
946 Cranwell, P., 1981. Diagenesis of free and bound lipids in terrestrial
947 detritus deposited in a lacustrine sediment. Org. Geochem. 3, 79-89.
948 Dayet, L., Texier, P.-J., Daniel, F., Porraz, G., 2013. Ochre resources from
949 the Middle Stone Age sequence of Diepkloof Rock Shelter, Western Cape, South
950 Africa. Journal of Archaeological Science 40, 3492-3505.
951 Del Rio, J.C., Hatcher, P.G., 1998. Analysis of aliphatic biopolymers using
952 thermochemolysis with tetramethylammonium hydroxide (TMAH) and gas
953 chromatography-mass spectrometry. Org. Geochem. 29, 1441-1451.
954 Dupont, L.M., Linder, H.P., Rommerskirchen, F., Schefuß, E., 2011.
955 Climate‐driven rampant speciation of the Cape flora. Journal of Biogeography
956 38, 1059-1068.
957 Eckmeier, E., Wiesenberg, G.L., 2009. Short-chain n-alkanes (C16–20) in
958 ancient soil are useful molecular markers for prehistoric biomass burning.
959 Journal of Archaeological Science 36, 1590-1596.
960 Eglinton, G., Hamilton, R.J., 1967. Leaf Epicuticular Waxes. Science 156,
961 1322-1335.

962 Eglinton, T.I., Eglinton, G., 2008. Molecular proxies for paleoclimatology.
963 Earth Planet. Sci. Lett. 275, 1-16.
964 Feakins, S.J., Sessions, A.L., 2010. Controls on the D/H ratios of plant leaf
965 waxes in an arid ecosystem. Geochim. Cosmochim. Acta 74, 2128-2141.
966 Feathers, J., 2015. Luminescence dating at Diepkloof Rock Shelter–new
967 dates from single-grain quartz. Journal of Archaeological Science 63, 164-174.
968 Fezzy, S., Armitage, R.A., 2006. Pyrolysis GC–MS and THM-GC–MS studies
969 of a black coating from Little Lost River Cave, Idaho. J. Anal. Appl. Pyrolysis 77,
970 102-110.
971 Goldberg, P., Miller, C.E., Schiegl, S., Ligouis, B., Berna, F., Conard, N.J.,
972 Wadley, L., 2009. Bedding, hearths, and site maintenance in the Middle Stone age
973 of Sibudu cave, KwaZulu-Natal, South Africa. Archaeological and Anthropological
974 Sciences 1, 95-122.
975 Goñi, M.A., Hedges, J.I., 1992. Lignin dimers: Structures, distribution, and
976 potential geochemical applications. Geochim. Cosmochim. Acta 56, 4025-4043.
977 Henshilwood, C.S., d'Errico, F., Yates, R., Jacobs, Z., Tribolo, C., Duller, G.A.,
978 Mercier, N., Sealy, J.C., Valladas, H., Watts, I., 2002. Emergence of modern human
979 behavior: Middle Stone Age engravings from South Africa. Science 295, 1278-
980 1280.
981 Hernandez‐Soriano, M.C., Kerré, B., Goos, P., Hardy, B., Dufey, J.,
982 Smolders, E., 2016. Long‐term effect of biochar on the stabilization of recent
983 carbon: soils with historical inputs of charcoal. GCB Bioenergy 8, 371-381.
984 Herrmann, N., Boom, A., Carr, A.S., Chase, B.M., Granger, R., Hahn, A., Zabel,
985 M., Schefuß, E., 2016. Sources, transport and deposition of terrestrial organic
986 material: A case study from southwestern Africa. Quat. Sci. Rev. 149, 215-229.

Herrmann, N., Boom, A., Carr, A.S., Chase, B.M., West, A.G., Zabel, M., Schefuß, E., 2017. Hydrogen isotope fractionation of leaf wax n-alkanes in southern African soils. Org. Geochem. 109, 1-13.

Hijmans, R.J., Cameron, S.E., Parra, J.L., Jones, P.G., Jarvis, A., 2005. Very high resolution interpolated climate surfaces for global land areas. International journal of climatology 25, 1965-1978.

Jacobs, Z., Roberts, R.G., 2015. An improved single grain OSL chronology for the sedimentary deposits from Diepkloof Rockshelter, Western Cape, South Africa. Journal of Archaeological Science 63, 175-192.

Jacobs, Z., Roberts, R.G., Galbraith, R.F., Deacon, H.J., Grün, R., Mackay, A., Mitchell, P., Vogelsang, R., Wadley, L., 2008. Ages for the Middle Stone Age of southern Africa: implications for human behavior and dispersal. Science 322, 733-735.

Kaal, J., Baldock, J.A., Buurman, P., Nierop, K.G., Pontevedra-Pombal, X., Martínez-Cortizas, A., 2007. Evaluating pyrolysis–GC/MS and 13C CPMAS NMR in conjunction with a molecular mixing model of the Penido Vello peat deposit, NW Spain. Org. Geochem. 38, 1097-1111.

Kaal, J., Cortizas, A.M., Nierop, K.G., 2009. Characterisation of aged charcoal using a coil probe pyrolysis-GC/MS method optimised for black carbon. J. Anal. Appl. Pyrolysis 85, 408-416.

Kaal, J., Rumpel, C., 2009. Can pyrolysis-GC/MS be used to estimate the degree of thermal alteration of black carbon? Org. Geochem. 40, 1179-1187.

Kaal, J., Schneider, M.P., Schmidt, M.W., 2012. Rapid molecular screening of black carbon (biochar) thermosequences obtained from chestnut wood and rice straw: A pyrolysis-GC/MS study. Biomass Bioenergy 45, 115-129.

1012 Mallol, C., Hernández, C.M., Cabanes, D., Sistiaga, A., Machado, J.,
1013 Rodríguez, Á., Pérez, L., Galván, B., 2013. The black layer of Middle Palaeolithic
1014 combustion structures. Interpretation and archaeostratigraphic implications.
1015 Journal of Archaeological Science 40, 2515-2537.
1016 Masiello, C.A., 2004. New directions in black carbon organic geochemistry.
1017 Mar. Chem. 92, 201-213.
1018 Miller, C.E., Goldberg, P., Berna, F., 2013. Geoarchaeological investigations
1019 at Diepkloof Rock Shelter, Western Cape, South Africa. Journal of Archaeological
1020 Science 40, 3432-3452.
1021 Milton, S.J., Yeaton, R.I., Dean, W.R.J., Vlok, J.H.J., 1997. Succulent Karoo, in:
1022 Cowling, R.W., Richardson, D.M., Pierce, S.M. (Eds.), Vegetation of Southern
1023 Africa. Cambridge University Press, Cambridge, pp. 131–166.
1024 Mizutani, H., Wada, E., 1985. High-performance liquid chromatographic
1025 determination of uric acid in soil. J. Chromatogr. A 331, 359-369.
1026 Nierop, K.G., van Bergen, P.F., 2002. Clay and ammonium catalyzed
1027 reactions of alkanols, alkanoic acids and esters under flash pyrolytic conditions.
1028 J. Anal. Appl. Pyrolysis 63, 197-208.
1029 Parkington, J., Poggenpoel, C., 1987. Diepkloof rock shelter, Papers in the
1030 prehistory of the western Cape, South Africa. Oxford: BAR International Series,
1031 pp. 269-293.
1032 Poole, I., Braadbaart, F., Boon, J.J., van Bergen, P.F., 2002. Stable carbon
1033 isotope changes during artificial charring of propagules. Org. Geochem. 33, 1675-
1034 1681.
1035 Porraz, G., Texier, P.-J., Archer, W., Piboule, M., Rigaud, J.-P., Tribolo, C.,
1036 2013. Technological successions in the Middle Stone Age sequence of Diepkloof

1037 Rock Shelter, Western Cape, South Africa. Journal of Archaeological Science 40,
1038 3376-3400.
1039 Poynter, J., Farrimond, P., Robinson, N., Eglinton, G., 1989. Aeolian-derived
1040 higher plant lipids in the marine sedimentary record: Links with palaeoclimate,
1041 Paleoclimatology and paleometeorology: modern and past patterns of global
1042 atmospheric transport. Springer, pp. 435-462.
1043 Rommerskirchen, F., Plader, A., Eglinton, G., Chikaraishi, Y., Rullkötter, J.,
1044 2006. Chemotaxonomic significance of distribution and stable carbon isotopic
1045 composition of long-chain alkanes and alkan-1-ols in C4 grass waxes. Org.
1046 Geochem. 37, 1303-1332.
1047 Rozanski, K., Araguás-Araguás, L., Gonfiantini, R., 1993. Isotopic patterns
1048 in modern global precipitation. In: Savin, S. (Eds.). Climate Change in Continental
1049 Isotopic Records. American Geophysical Union, Washington, DC, pp. 1–36.
1050 Rundel, P.W., Esler, K.J., Cowling, R.M., 1999. Ecological and phylogenetic
1051 patterns of carbon isotope discrimination in the winter-rainfall flora of the
1052 Richtersveld, South Africa. Plant Ecology 142, 133-148.
1053 Rutherford, M.C., Mucina, L., Powrie, L.W., 2006. Biomes and Bioregions of
1054 Southern Africa. , in: Mucina, L., Rutherford, M.C. (Eds.), The vegetation of South
1055 Africa, Lesotho and Swaziland. South African National Biodiversity Institute,
1056 Pretoria, pp. 30-51.
1057 Sachse, D., Billault, I., Bowen, G.J., Chikaraishi, Y., Dawson, T.E., Feakins,
1058 S.J., Freeman, K.H., Magill, C.R., McInerney, F.A., van der Meer, M.T.J., Polissar, P.,
1059 Robins, R.J., Sachs, J.P., Schmidt, H.-L., Sessions, A.L., White, J.W.C., West, J.B.,
1060 Kahmen, A., 2012. Molecular Paleohydrology: Interpreting the Hydrogen-Isotopic

1061 Composition of Lipid Biomarkers from Photosynthesizing Organisms. Annual
1062 Review of Earth and Planetary Sciences 40, 221-249.
1063 Sáiz-Jiménez, C., 1994. Analytical pyrolysis of humic substances: pitfalls,
1064 limitations, and possible solutions. Environmental science & technology 28,
1065 1773-1780.
1066 Sáiz-Jiménez, C., De Leeuw, J., 1986. Chemical characterization of soil
1067 organic matter fractions by analytical pyrolysis-gas chromatography-mass
1068 spectrometry. J. Anal. Appl. Pyrolysis 9, 99-119.
1069 Schefuß, E., Ratmeyer, V., Stuut, J.-B.W., Jansen, J.H.F., Sinninghe Damsté,
1070 J.S., 2003. Carbon isotope analyses of *n*-alkanes in dust from the lower
1071 atmosphere over the central eastern Atlantic. Geochim. Cosmochim. Acta 67,
1072 1757-1767.
1073 Sealy, J.C., Van Der Merwe, N.J., Thorp, J.A.L., Lanham, J.L., 1987. Nitrogen
1074 isotopic ecology in southern Africa: implications for environmental and dietary
1075 tracing. Geochim. Cosmochim. Acta 51, 2707-2717.
1076 Simoneit, B.R., 2002. Biomass burning—a review of organic tracers for
1077 smoke from incomplete combustion. Appl. Geochem. 17, 129-162.
1078 Steele, T.E., Klein, R.G., 2013. The Middle and Later Stone Age faunal
1079 remains from Diepkloof Rock Shelter, Western Cape, South Africa. Journal of
1080 Archaeological Science 40, 3453-3462.
1081 Stock, W., Wienand, K., Baker, A., 1995. Impacts of invading N2-fixing
1082 Acacia species on patterns of nutrient cycling in two Cape ecosystems: evidence
1083 from soil incubation studies and 15N natural abundance values. Oecologia 101,
1084 375-382.

1085 Szpak, P., Millaire, J.-F., White, C.D., Longstaffe, F.J., 2012. Influence of
1086 seabird guano and camelid dung fertilization on the nitrogen isotopic
1087 composition of field-grown maize (Zea mays). Journal of Archaeological Science
1088 39, 3721-3740.
1089 Texier, P.-J., Porraz, G., Parkington, J., Rigaud, J.-P., Poggenpoel, C., Miller,
1090 C., Tribolo, C., Cartwright, C., Coudenneau, A., Klein, R., 2010. A Howiesons Poort
1091 tradition of engraving ostrich eggshell containers dated to 60,000 years ago at
1092 Diepkloof Rock Shelter, South Africa. Proceedings of the National Academy of
1093 Sciences 107, 6180-6185.
1094 Texier, P.-J., Porraz, G., Parkington, J., Rigaud, J.-P., Poggenpoel, C., Tribolo,
1095 C., 2013. The context, form and significance of the MSA engraved ostrich eggshell
1096 collection from Diepkloof Rock Shelter, Western Cape, South Africa. Journal of
1097 Archaeological Science 40, 3412-3431.
1098 Thevenot, M., Dignac, M.-F., Rumpel, C., 2010. Fate of lignins in soils: a
1099 review. Soil Biol. Biochem. 42, 1200-1211.
1100 Trabucco, A., Zomer, R.J., 2009. Global Potential Evapo-Transpiration
1101 (Global-PET) and Global Aridity Index (Global-Aridity) Geo-Database. CGIAR
1102 Consortium for Spatial Information. Available online from the CGIAR-CSI
1103 GeoPortal at: http://www.csi.cgiar.org.
1104 Tribolo, C., Mercier, N., Douville, E., Joron, J.-L., Reyss, J.-L., Rufer, D.,
1105 Cantin, N., Lefrais, Y., Miller, C., Porraz, G., 2013. OSL and TL dating of the Middle
1106 Stone Age sequence at Diepkloof Rock Shelter (South Africa): a clarification.
1107 Journal of Archaeological Science 40, 3401-3411.
1108 Tribolo, C., Mercier, N., Valladas, H., Joron, J.-L., Guibert, P., Lefrais, Y., Selo,
1109 M., Texier, P.-J., Rigaud, J.-P., Porraz, G., 2009. Thermoluminescence dating of a

1110 Stillbay–Howiesons Poort sequence at Diepkloof Rock Shelter (Western Cape,
1111 South Africa). Journal of Archaeological Science 36, 730-739.
1112 Vancampenhout, K., Wouters, K., Caus, A., Buurman, P., Swennen, R.,
1113 Deckers, J., 2008. Fingerprinting of soil organic matter as a proxy for assessing
1114 climate and vegetation changes in last interglacial palaeosols (Veldwezelt,
1115 Belgium). Quaternary Research 69, 145-162.
1116 Vogel, J.C., Fuls, A., Ellis, R.P., 1978. Geographical distribution of Kranz
1117 grasses in South Africa. S. Afr. J. Sci.
1118 Vogts, A., Moossen, H., Rommerskirchen, F., Rullkötter, J., 2009.
1119 Distribution patterns and stable carbon isotopic composition of alkanes and
1120 alkan-1-ols from plant waxes of African rain forest and savanna C_3 species. Org.
1121 Geochem. 40, 1037-1054.
1122 Wadley, L., 2015. Those marvellous millennia: the Middle Stone Age of
1123 Southern Africa. Azania: Archaeological Research in Africa 50, 155-226.
1124 Wadley, L., Sievers, C., Bamford, M., Goldberg, P., Berna, F., Miller, C., 2011.
1125 Middle Stone Age bedding construction and settlement patterns at Sibudu, South
1126 Africa. Science 334, 1388-1391.
1127 Wiesenberg, G., Lehndorff, E., Schwark, L., 2009. Thermal degradation of
1128 rye and maize straw: lipid pattern changes as a function of temperature. Org.
1129 Geochem. 40, 167-174.
1130
1131
1132
1133
1134